JAEA-Research
2010-053

JAEA-Research

Deduced Soft-rotator Model Hamiltonian Parameters and Collective Properties of Medium-to-heavy Even-even Nuclei

Satoshi KUNIEDA, Satoshi CHIBA, Keiichi SHIBATA, Akira ICHIHARA
Osamu IWAMOTO, Nobuyuki IWAMOTO, Tokio FUKAHORI
and Efrem Sh. SUKHOVITSKIĬ

Division of Nuclear Data and Reactor Engineering
Nuclear Science and Engineering Directorate

February 2011

Japan Atomic Energy Agency

日本原子力研究開発機構

独立行政法人日本原子力研究開発機構　研究技術情報部　研究技術情報課
〒319-1195　茨城県那珂郡東海村白方白根 2 番地 4
電話 029-282-6387, Fax 029-282-5920, E-mail:ird-support@jaea.go.jp

JAEA-Research 2010-053

Deduced Soft-rotator Model Hamiltonian Parameters and Collective Properties of Medium-to-heavy Even-even Nuclei

Satoshi KUNIEDA, Satoshi CHIBA, Keiichi SHIBATA, Akira ICHIHARA,
Osamu IWAMOTO, Nobuyuki IWAMOTO, Tokio FUKAHORI
and Efrem Sh. SUKHOVITSKIĬ*

Division of Nuclear Data and Reactor Engineering
Nuclear Science and Engineering Directorate
Japan Atomic Energy Agency, Tokai-mura, Naka-gun, Ibaraki-ken

(Received December 3, 2010)

The soft-rotator model Hamiltonian parameters were deduced for 63 even-even medium and heavy nuclei in a mass range $56 \leq A \leq 238$. We obtained those values by the combination of the low-lying level structure and the coupled-channels proton scattering analyses. It was found that the values of the effective quadrupole and octupole deformations obtained were consistent with those derived from experimental data. Besides, the equilibrium ground-state quadrupole deformation parameters were also in reasonable accord with the theoretical mass-models results for deformed heavy nuclei. In this report, we present a complete set of the Hamiltonian parameters for each nucleus. The obtained values of the parameters often varied with the constituent neutron and/or proton numbers anomalously. On the other hand, some clear systematic trends were seen among the major Hamiltonian parameters.

Keywords: Soft-rotator Model, Coupled-channels Optical Model, Collective Nature, Hamiltonian Parameters, Even-even Nuclei, Medium and Heavy Nuclei, Low-lying Level Structure, Proton Inelastic Scattering, Anomalous Behaviors, Systematic Trends

*Joint Institute for Energy and Nuclear Research, 220109, Minsk-Sosny, Belarus

比較的重い偶-偶核に対する軟回転体模型ハミルトニアンパラメータの推定値と集団的性質

日本原子力研究開発機構　原子力基礎工学研究部門　核工学・炉工学ユニット
国枝　賢、千葉　敏、柴田　恵一、市原　晃、岩本 修、
岩本　信之、深堀　智生、Efrem Sh. SUKHOVITSKIĬ*

(2010 年 12 月 3 日受理)

質量数 56 から 238 までの中重核領域における 63 種の偶-偶核に対して軟回転体模型ハミルトニアンパラメータを導出した。パラメータの値は、軟回転体模型による離散励起レベル構造の解析およびチャネル結合光学模型による陽子非散乱微分断面積の解析を同時に行って推定した。得られた実効的な四重極および八重極変形の値は測定値に基づく結果と比べて大きな矛盾が無く、重核の基底変形パラメータは原子核質量モデルによる理論計算結果と比較的良く一致した。このレポートでは核種毎に完全なハミルトニアンパラメータセットを示す。原子核の中性子数や陽子数が異なるごとにパラメータの値が不規則に変化するケースが多々見られたが、主要なパラメータ間には明らかな相関が見られた。

原子力科学研究所（駐在）: 〒 319-1195 茨城県那珂郡東海村白方白根 2-4
*エネルギー及び原子核共同研究所（ベラルーシ）

Contents

目次

List of Tables

List of Figures

This is a blank page.

1 Introduction

An atomic nucleus has its own character which is ascribed to the difference of the constituent neutron and/or proton numbers. It is not easy to explicitly predict even the macroscopic nature of a nucleus because it usually shows irregular behaviors. For instance, the shape transitional regions are well known to exist at around relatively narrow mass-ranges, e.g., $82 \lesssim N \lesssim 92$, where collective properties rapidly change from the typical vibrational to the rotational one. Quantitative knowledge of those behaviors should give an essential step for us to recognize and predict the individuality of the nucleus. In addition to such physical interest, our motivation was also triggered by an engineering purpose, i.e., the nuclear data evaluation. The phenomenological nuclear (reaction) models are usually employed to predict/evaluate such data as the particle scattering and the varieties of reaction cross sections. In order to obtain reliable data, it is an important "key" to describe the collective nature of the target nucleus appropriately in the model calculations.

The nuclear collective excitation is one of the general phenomena in which a nucleus shows its own coherent properties. Recently, the soft-rotator model[1, 2] (SRM) analysis has succeeded in description of the low-lying levels and collective natures for some even-even nuclei. At the same time, the coupled-channels (CC) optical model analyses have also been done based on the nuclear properties described by the SRM (SRM-CC), which resulted in successful nucleon-nucleus interaction studies. For instance, they are reported by Chiba *et al.* for ^{12}C[1, 3], by Sukhovitskiĩ *et al.* for ^{58}Ni[4], ^{56}Fe[5], ^{52}Cr[6] and by Sun *et al.* for ^{28,30}Si[7]. The model assumes that each nucleus has its own shape at the ground- and excited-states, and collective excitations are ascribed to the rotational-vibrational motion. It is the substantial feature of SRM that such concepts are considered for the quadrupole, octupole and hexadecapole modes. The model is expected to be applicable to the analyses for various rotational-vibrational even-even nuclei. Also, the findings to be obtained should give us extensive and useful knowledge for the characteristics of nuclei.

The main purposes of this study is to deduce a complete SRM Hamiltonian parameters for various even-even nuclei in order to quantitatively know their major collective properties within the framework of SRM. The analysis procedure basically follows the previous (original) studies referred in the preceding paragraph. Those parameters such as the axial and the non-axial equilibrium ground-state (G.S.) deformation and the softness of the surface vibrations are determined by the combination of the SRM level structure and the SRM-CC proton scattering analyses. In this work[†], we carry out those analyses for medium and heavy nuclides of which experimental data are available for both collective-excitation levels and inelastic proton scattering cross sections, i.e., 63 even-even nuclei such as ^{56,58}Fe, ^{60,62,64}Ni, $^{64-70}$Zn, $^{70-76}$Ge, $^{74-82}$Se, ^{86}Sr, ^{96,98,100}Mo, ^{102}Ru, $^{104-110}$Pd, $^{106-116}$Cd, $^{116-124}$Sn, $^{122-130}$Te, ^{144,150}Nd, $^{148-154}$Sm, ^{160}Gd, ^{164}Dy, ^{166,168}Er, ^{174,176}Yb, ^{178,180}Hf, ^{182,184}W, ^{192}Os, ^{194}Pt, ^{232}Th and ^{238}U. The obtained parameters are presented for each nucleus completely in this paper. The

[†]This work has already been overviewed in Ref.[8], and partially reported in Ref.[9]. We would like to devote this report to ones who want to know detailed numerical results.

deduced values of the deformation parameters are also compared with experimental data and major theoretical mass-model results in order to investigate the validity of our results. It is another purpose of this study to point out/discuss some notable isotopic differences, and to investigate systematic trends of the major Hamiltonian parameters.

This report is organized as follows. In Chap. 2, SRM and the model parameters are briefly described. We present our general approaches for the SRM Hamiltonian parameter-search in Chap. 3. The obtained parameters are given in Chap. 4. They are compared with experimental and various mass-model predictions in this chapter. Also, this chapter is devoted to discussions of their isotopic differences, notable behaviors, and systematic trends. Finally, Chap. 5 summarizes and concludes this study.

2 Brief Descriptions of the Soft-rotator Model and the Hamiltonian Parameters

The SRM was adopted in order to express the general feature of the low-lying collective states. The model originated from the Davydov-Chaban model[10] which was formulated to describe the quadrupole rotational-vibrational collective motion for non-axially deformed nuclei. The same concept had been applied to the octupole and hexadecapole properties by Porodzinskiĭ and Sukhovitskiĭ[11, 12]. The model and those concepts had been integrated into one, i.e., SRM, aiming to give general description of low-lying collective level structure for even-even nuclide. The detailed expressions of the model are given elsewhere[1, 2], so we would briefly describe its features and the model parameters in this section.

The model assumes that the nucleus has a non-spherical shape, which is characterized by the non-axial quadrupole, octupole and hexadecapole deformations. These deformations are considered to be ascribed to the collective excitations and the intrinsic deformation at the ground state. The nuclear shape is expressed in a body-fixed system (θ', ϕ') as follows.

$$\begin{aligned} R(\theta',\phi') &= R_0\Big\{1+\sum_{\lambda\mu}\beta_{\lambda\mu}Y_{\lambda\mu}(\theta',\phi')\Big\} \\ &= R_0\Bigg\{1+\beta_2\Big[\cos\gamma Y_{20}(\theta',\phi')+\frac{1}{2}\sin\gamma\Big((Y_{22}(\theta',\phi')+Y_{2-2}(\theta',\phi')\Big)\Big] \\ &+ \beta_3\Big[\cos\eta Y_{30}(\theta',\phi')+\frac{1}{2}\sin\eta\Big((Y_{32}(\theta',\phi')+Y_{3-2}(\theta',\phi')\Big)\Big] \\ &+ b_{40}Y_{40}(\theta',\phi')+\sum_{\mu=2,4}b_{4\mu}\Big(Y_{4\mu}(\theta',\phi')+Y_{4-\mu}(\theta',\phi')\Big)\Bigg\}, \end{aligned} \tag{1}$$

where,

$$b_{40} = \beta_4\left(\sqrt{\frac{7}{12}}\cos\delta_4+\sqrt{\frac{5}{12}}\sin\delta_4\cos\gamma_4\right), \tag{2}$$

$$b_{42} = -\beta_4\sqrt{\frac{1}{2}}\sin\delta_4\sin\gamma_4, \tag{3}$$

$$b_{44} = \beta_4\sqrt{\frac{1}{2}}\left(\sqrt{\frac{5}{12}}\cos\delta_4-\sqrt{\frac{7}{12}}\sin\delta_4\cos\gamma_4\right). \tag{4}$$

The symbol $\beta_\lambda(=\sqrt{\sum_\mu\beta_{\lambda\mu}\beta^*_{\lambda\mu}})$ denotes the variable for deformation with multipolarity $\lambda(=2,3)$, while the value of β_4 is treated as a constant (static deformation). The non-axialities are represented by the variable γ for quadrupole, by constant values η for octupole, δ_4 and γ_4 for hexadecapole deformations. The Hamiltonian for the collective motions is assumed to be written as,

$$\hat{H}=\frac{\hbar^2}{2}\left\{\hat{T}_{\rm rot.}+\frac{1}{B_2}\Big[\hat{T}_{\beta_2}+\frac{1}{\beta_2^2}\hat{T}_\gamma\Big]+\frac{1}{B_3}\hat{T}_{\beta_3}\right\}+V(\beta_2)+V(\beta_3)+\frac{\beta_{20}^4}{\beta_2^2}V(\gamma), \tag{5}$$

where the vibrational energy operators are expressed as

$$\hat{T}_{\beta_2} = -\frac{1}{\beta_2^4}\frac{\partial}{\partial\beta_2}\left(\beta_2^4\frac{\partial}{\partial\beta_2}\right), \tag{6}$$

$$\hat{T}_{\gamma} = -\frac{1}{\sin 3\gamma}\frac{\partial}{\partial\gamma}\left(\sin 3\gamma\frac{\partial}{\partial\gamma}\right), \tag{7}$$

$$\hat{T}_{\beta_3} = -\frac{1}{\beta_3^3}\frac{\partial}{\partial\beta_3}\left(\beta_3^3\frac{\partial}{\partial\beta_3}\right), \tag{8}$$

for the quadrupole (β_2-), γ- and octupole (β_3-) motions, respectively. The potential energies $V(\beta_2)$, $V(\gamma)$ and $V(\beta_3)$ correspond to those for such vibrations. Since the hexadecapole vibrational property is very weak in general, it was not considered here. The symbol $\hat{T}_{\rm rot.}$ stands for the operator for the rotational energy. It is formulated with the projection of the angular momentum operator on i-th axis of the body-fixed system $\hat{I}_i$, and the principal moments of inertia in direction of the i-th axis $J_i^{(\lambda)}$:

$$\hat{T}_{\rm rot.} = \sum_{i=1}^{3}\frac{\hat{I}_i^2}{J_i^{(2)}+J_i^{(3)}+J_i^{(4)}}. \tag{9}$$

The values of $J_i^{(\lambda)}$ are calculated taking account of the non-axial deformations as,

$$J_i^{(2)} = 4B_2\beta_2^2\sin^2(\gamma-2/3\pi i), \tag{10}$$

$$J_1^{(3)} = 4B_3\beta_3^2\left(\frac{1}{2}\cos^2\eta+\frac{\sqrt{15}}{4}\sin 2\eta+1\right), \tag{11}$$

$$J_2^{(3)} = 4B_3\beta_3^2\left(\frac{1}{2}\cos^2\eta-\frac{\sqrt{15}}{4}\sin 2\eta+1\right), \tag{12}$$

$$J_3^{(3)} = 4B_3\beta_3^2\sin^2\eta, \tag{13}$$

$$J_1^{(4)} = 4B_4\left(\frac{5}{2}b_{40}^2+4b_{42}^2+b_{44}^2+\frac{3}{2}\sqrt{10}b_{40}b_{42}+\sqrt{7}b_{42}b_{44}\right), \tag{14}$$

$$J_2^{(4)} = 4B_4\left(\frac{5}{2}b_{40}^2+4b_{42}^2+b_{44}^2-\frac{3}{2}\sqrt{10}b_{40}b_{42}-\sqrt{7}b_{42}b_{44}\right), \tag{15}$$

$$J_3^{(4)} = 4B_4(2b_{42}^2+8b_{44}^2), \tag{16}$$

where the symbol B_λ ($\lambda=2,3,4$) represents the mass parameter. In the present model, an octupole deformation variable β_3 is treated as $\beta_3=\epsilon\beta_2$, assuming it behaves in direct proportion to β_2 owing to centrifugal forces caused by the rotation. The excited energies are obtained as the eigenvalues of the Hamiltonian $\hat{H}$.

Generally, fourteen parameters are required in order to give a complete description of the Hamiltonian. Most of them can be estimated by the phenomenological way, namely, the low-lying level structure analysis. The softness parameters $\mu_{\beta_{20}}$, μ_ϵ and μ_{γ_0} are introduced to describe strengths of the vibrations, i.e., the vibrational potential energies such as $V(\beta_2)$, $V(\beta_3)$ and $V(\gamma)$, respectively. As for the octupole vibration, the excited energies are calculated by

$$E_{n_{\beta_3}}^{\pm} = \frac{\hbar^2}{B_3\mu_\epsilon^2}\left(n_{\beta_3}+\frac{1}{2}\right)\mp\delta_n, \qquad (n_{\beta_3}=0,1,2,\cdots). \tag{17}$$

In this model, the octupole deformed nucleus is considered to have two minima of the potential energy which correspond with two symmetric octupole shape. The value of $2\delta_n$ denotes the splitting

energy for a double-levels generation caused by the tunneling effect. The quadrupole, quadrupole-γ and octupole deformation parameters, such as β_{20}, γ_0 and $\epsilon_0\beta_{20}(=\beta_{30})$ should be given as the equilibrium deformations. The hexadecapole deformation parameter β_4, the non-axiality parameters η, δ_4 and γ_4 are assumed to be static (constant). The quadrupole mass-parameter is treated as one of the components of an over all scale factor $\hbar\omega_0$ for level energies to be calculated : $\hbar\omega_0 = \hbar^2/B_2\mu^2_{\beta_{20}}\beta^2_{20}$. The octupole and hexadecapole parameters are also treated as relative ones to the quadrupole value as $a_{32} = (B_3/B_2)(\beta_{30}/\beta_{20})^2$, and $a_{42} = (B_4/B_2)(\beta_4/\beta_{20})^2$. Once again, let us summarize the SRM Hamiltonian parameters : the overall scale factor $\hbar\omega_0$, the quadrupole parameters $\mu_{\beta_{20}}$, μ_{γ_0}, β_{20}, γ_0, the octupole parameters μ_ϵ, ϵ_0, η, a_{32}, δ_n and the hexadecapole parameters β_4, δ_4, γ_4, a_{42}.

3 Parameter Search

3.1 Level Structure Analysis

3.1.1 Analysis Procedure

The SRM Hamiltonian parameters were derived from the experimentally-known level data by phenomenological analyses for each nucleus. Namely, we determined these parameters to give a good description of the measured level data by the model calculation. The parameter values to be obtained enable us to describe a complete SRM Hamiltonian for each nucleus. The SHEMMAN code[2] allowed us to carry out the model computations. In this analysis, it was essential for us to know the band structure in advance, involving the G.S., the non-axial (γ-), the quadrupole-vibrational (β_2-) and the octupole negative-parity (β_3-) bands. It is not difficult to identify such major bands for the typical deformed heavy nuclei because their low-lying collective properties are clearly characterized by the rotation accompanied by the vibration (so-called rotational bands). Actually, their band structures had been measured/evaluated over the ages, and now, they are well known as compiled in the series of Nuclear Data Sheets[‡]. For transitional and typical vibrational nuclei, however, the band structure has not been identified in many cases. It was just because their collective natures involved a complex of various types of vibrations and rotations. Thus for those nuclei, we were enforced to empirically assign each low-lying level to one of the members of a "plausible" band though the values of level energy, spin and parity were taken from the latest version of Nuclear Data Sheets. So we have to admit this procedure may bring an ambiguity to the analyses and the results to be obtained. But we would like to emphasize that the final judgements of the band identifications were done after confirming the best combination of the assumed level structure, the SRM parameter set and the calculated levels which gave the least-square deviation. Also, in order to reduce such uncertainties and to do analyses under a systematic manner, we just considered the primary bands, i.e., the G.S. band with ($\tau = 1$, $n_\gamma = 0$, $n_{\beta_2} = 0$, $n_{\beta_3} = 0$), the γ-band with ($\tau = 2$, $n_\gamma = 0$, $n_{\beta_2} = 0$, $n_{\beta_3} = 0$), β_2-band with ($\tau = 1$, $n_\gamma = 0$, $n_{\beta_2} = 1$, $n_{\beta_3} = 0$) and β_3-band with ($\tau = 1$, $n_\gamma = 0$, $n_{\beta_2} = 0$, $n_{\beta_3} = 0$) where the quantities in the parentheses denote quantum numbers in SRM. The band structure was determined/assumed under following pictures for each band.

- ▷ Ground-state band ($\tau = 1$, $n_\gamma = 0$, $n_{\beta_2} = 0$, $n_{\beta_3} = 0$) :
  The first 0^+ (ground-state), the first 2^+ and 4^+ states were always treated as members of this band. If succeeding 6^+, 8^+ and 10^+ levels existed in the expected position, or identified as ones of G.S. band in the Nuclear Data Sheets, they were adopted as the members of this family. These levels may be excited not only by the rotation but also by the zero-point β-vibrations.

- ▷ γ-band ($\tau = 2$, $n_\gamma = 0$, $n_{\beta_2} = 0$, $n_{\beta_3} = 0$) :
  This band data are indispensable to deduce the non-axial parameters. A series of positive levels 2^+, 3^+, 4^+, $\cdots$ is known to correspond to this band for even-even isotopes. Though the band is

[‡]Their references are listed in a recent publication.

given for many deformed heavy nuclei in Nuclear Data Sheets, it is not tightly identified in general particularly for the light and the medium nuclides. So we were enforced to determine this band empirically for many isotopes. It is a fortunate fact that one of the distinctive properties of this family is the existence of 3^+ state. It is an infrequent level among the low-lying discrete levels, thus we always assigned the first 3^+ level to a member of this band. If there existed 2^+ state below and 4^+ above it, they were the candidates for this family.

▷ β_2-vibrational band ($\tau = 1$, $n_\gamma = 0$, $n_{\beta_2} = 1$, $n_{\beta_3} = 0$) :
This is the quadrupole-vibrational band with the second quantum number $n_{\beta_2} = 1$. The members are known to have J^π of 0^+, 2^+, 4^+, $\cdots$. Though it is difficult to ensure our identification, we always assumed the second 0^+ is the family of this band in this study. The succeeding 2^+, 4^+, 6^+, $\cdots$ levels should be the candidates of this band.

▷ Octupole negative-parity band ($\tau = 1$, $n_\gamma = 0$, $n_{\beta_2} = 0$, $n_{\beta_3} = 0$) :
In general, it is known that the first 3^- state tends to show a strong collectivity especially for the spherical (hard) nuclei. We considered this level as a member of this band without exceptions. If there existed 1^- and/or 5^- near the first 3^- level, they were also treated as members of this family.

The adopted levels and the assumed band structure are listed in **Table 1** for each nucleus.

Table 1: The experimental levels (identified by J^π and excitation energy in keV) and the band structure for each isotopes which were assumed in the present SRM level structure analyses. The calculated level energies are also given between parentheses.

- ^{56}Fe -

G. S. band			γ-band			β_2-band			Octupole band		
[c] 0^+	0.0	(0.0)	2^+	2657.5	(2713.5)	0^+	2941.7	(2923.6)			
[c] 2^+	846.8	(805.3)	3^+	3445.3	(3305.1)	2^+	3748.0	(3755.5)	[c] 3^-	4510.0	(4364.8)
[c] 4^+	2085.1	(2190.0)							5^-	5122.1	(5322.7)
6^+	3755.6	(3861.0)									

- ^{58}Fe -

G. S. band†			γ-band			β_2-band			Octupole band		
[c] 0^+	0.0	(0.0)	2^+	1674.8	(1610.9)	0^+	2258.0	(2215.2)			
[c] 2^+	810.8	(808.3)	3^+	2133.9	(2252.0)	2^+	2876.5	(2973.8)	[c] 3^-	3860.8	(3814.7)
[c] 4^+	2076.5	(2010.1)									
6^+	3596.9	(3633.0)									

- ^{60}Ni -

G. S. band			γ-band			β_2-band			Octupole band		
[c] 0^+	0.0	(0.0)	2^+	2158.6	(2096.4)	0^+	2284.9	(2257.3)			
[c] 2^+	1332.5	(1297.7)	3^+	2626.1	(2757.3)				[c] 3^-	4039.7	(4029.3)

table continued on next page

continued from previous page

[c] 4^+	2505.8	(2545.2)									

- ^{62}Ni -

G. S. band			γ-band			β_2-band			Octupole band		
[c] 0^+	0.0	(0.0)	2^+	3157.7	(3143.0)	0^+	2048.6	(2103.7)			
[c] 2^+	1172.9	(1119.5)	3^+	3552.7	(3542.2)	2^+	3518.5	(3475.9)	[c] 3^-	3757.0	(3715.8)
[c] 4^+	2336.3	(2418.5)									

- ^{64}Ni -

G. S. band			γ-band			β_2-band			Octupole band		
[c] 0^+	0.0	(0.0)	2^+	2276.6	(2241.6)	0^+	2867.3	(2819.1)			
[c] 2^+	1345.8	(1301.7)							[c] 3^-	3560.4	(3580.1)
[c] 4^+	2610.1	(2751.0)									

- ^{64}Zn -

G. S. band[†]			γ-band			β_2-band			Octupole band[†]		
[c] 0^+	0.0	(0.0)	2^+	1799.4	(1885.3)	0^+	1910.3	(1911.7)			
[c] 2^+	991.5	(972.8)	3^+	2979.8	(2584.6)	2^+	2793.8	(2811.8)	[c] 3^-	2998.4	(3010.0)
[c] 4^+	2306.7	(2289.4)									
6^+	3993.4	(3994.3)									

- ^{66}Zn -

G. S. band			γ-band			β_2-band			Octupole band		
[c] 0^+	0.0	(0.0)	2^+	1872.8	(1892.5)	0^+	2372.4	(2342.0)			
[c] 2^+	1039.2	(1022.9)	3^+	2703.6	(2635.8)	2^+	3212.6	(3270.7)	[c] 3^-	2826.7	(2796.2)
[c] 4^+	2451.0	(2410.1)							5^-	3747.0	(3805.9)
6^+	4182.7	(4240.6)									

- ^{68}Zn -

G. S. band[†]			γ-band			β_2-band			Octupole band		
[c] 0^+	0.0	(0.0)	2^+	1883.2	(2039.2)	0^+	1655.9	(1500.5)			
[c] 2^+	1077.4	(1058.1)	3^+	3009.3	(2588.7)	2^+	2338.4	(2677.1)	[c] 3^-	2750.8	(2630.0)
[c] 4^+	2417.4	(2271.1)							5^-	3458.8	(3511.9)
6^+	3687.5	(3602.5)									

- ^{70}Zn -

G. S. band[†]			γ-band			β_2-band			Octupole band		
[c] 0^+	0.0	(0.0)	2^+	1758.8	(1903.0)	0^+	1070.2	(1081.1)			
[c] 2^+	884.5	(823.2)	3^+	2949.2	(2282.7)	2^+	1957.2	(2025.1)	[c] 3^-	2859.0	(2699.9)
[c] 4^+	1786.3	(1778.2)				4^+	2977.8	(2924.1)	5^-	3037.6	(3275.7)
6^+	2894.7	(2781.3)									

- ^{70}Ge -

G. S. band[†]			γ-band			β_2-band			Octupole band[†]		
[c] 0^+	0.0	(0.0)	2^+	1707.6	(1775.3)	0^+	1215.5	(1197.3)			
[c] 2^+	1039.5	(966.8)	3^+	2451.3	(2323.7)	2^+	2156.7	(2245.1)	[c] 3^-	2562.0	(2584.1)
[c] 4^+	2153.2	(2213.8)	4^+	3194.2	(3193.6)						

table continued on next page

continued from previous page

6^+	3297.1	(3321.3)									

- ^{72}Ge -

G. S. band			γ-band			β_2-band			Octupole band		
[c] 0^+	0.0	(0.0)	2^+	1464.0	(1484.3)	0^+	691.4	(715.0)			
[c] 2^+	834.0	(769.1)	3^+	2064.9	(1919.3)				[c] 3^-	2514.8	(2500.7)
[c] 4^+	1728.3	(1844.8)	4^+	2463.9	(2401.6)						
6^+	2772.1	(2909.1)									

- ^{74}Ge -

G. S. band†			γ-band			β_2-band			Octupole band		
[c] 0^+	0.0	(0.0)	2^+	1204.2	(1242.9)	0^+	1482.8	(1509.0)			
[c] 2^+	595.9	(609.0)	3^+	1697.1	(1618.8)	2^+	2197.9	(2150.0)	[c] 3^-	2536.3	(2581.7)
[c] 4^+	1463.8	(1425.5)									

- ^{76}Ge -

G. S. band			γ-band			β_2-band			Octupole band		
[c] 0^+	0.0	(0.0)	2^+	1108.4	(1113.2)	0^+	1911.1	(1874.7)			
[c] 2^+	562.9	(563.1)	3^+	1539.5	(1527.2)	2^+	2503.6	(2516.7)	[c] 3^-	2692.4	(2583.5)
[c] 4^+	1410.1	(1364.8)							5^-	2962.2	(3194.4)

- ^{74}Se -

G. S. band†			γ-band			β_2-band			Octupole band†		
[c] 0^+	0.0	(0.0)	2^+	1269.0	(1322.6)	0^+	853.8	(925.7)			
[c] 2^+	634.8	(628.1)	3^+	1884.3	(1636.6)	2^+	1838.7	(1633.1)	[c] 3^-	2349.7	(2345.6)
[c] 4^+	1363.2	(1395.4)							5^-	2842.6	(2850.2)
6^+	2231.4	(2249.6)									
8^+	3198.4	(3253.3)									

- ^{76}Se -

G. S. band†			γ-band†			β_2-band			Octupole band†		
[c] 0^+	0.0	(0.0)	2^+	1216.1	(1260.0)	0^+	1122.3	(1150.6)			
[c] 2^+	559.1	(566.5)	3^+	1689.0	(1603.2)	2^+	1787.6	(1764.8)	[c] 3^-	2429.1	(2332.3)
[c] 4^+	1330.9	(1316.7)	4^+	2026.0	(2075.0)				5^-	2824.8	(2890.3)
6^+	2262.4	(2230.5)	5^+	2489.3	(2434.7)						
8^+	3269.8	(3336.8)									

- ^{78}Se -

G. S. band†			γ-band†			β_2-band			Octupole band†		
[c] 0^+	0.0	(0.0)	2^+	1308.6	(1325.9)	0^+	1498.6	(1442.9)			
[c] 2^+	613.7	(605.5)	3^+	1853.9	(1748.4)	2^+	1995.9	(2062.7)	[c] 3^-	2507.3	(2423.4)
[c] 4^+	1502.8	(1457.4)	4^+	2190.7	(2364.5)				5^-	2889.9	(2960.2)
6^+	2546.5	(2530.5)	5^+	2735.0	(2775.4)						
8^+	3585.0	(3564.5)									

- ^{80}Se -

G. S. band†			γ-band			β_2-band			Octupole band		

table continued on next page

continued from previous page

[c] 0^+	0.0	(0.0)	2^+	1449.3	(1522.8)	0^+	1478.8	(1496.2)			
[c] 2^+	666.3	(696.5)	3^+	2121.1	(1972.8)	2^+	2311.3	(2225.1)	[c] 3^-	2716.7	(2785.8)
[c] 4^+	1701.5	(1650.0)									
6^+	2895.5	(2865.0)									

- ^{82}Se -

G. S. band			γ-band			β_2-band			Octupole band		
[c] 0^+	0.0	(0.0)	2^+	1731.5	(1841.1)	0^+	1410.3	(1389.2)			
[c] 2^+	654.8	(669.5)	3^+	2550.3	(2280.9)				[c] 3^-	3009.2	(2663.7)
[c] 4^+	1735.1	(1697.2)							5^-	2893.7	(3364.7)
6^+	3145.0	(2988.3)									

- ^{86}Sr -

G. S. band			γ-band			β_2-band			Octupole band		
[c] 0^+	0.0	(0.0)	2^+	1854.2	(1848.4)	0^+	2106.0	(2095.9)			
[c] 2^+	1076.7	(1074.6)							[c] 3^-	2481.9	(2490.8)
4^+	2229.7	(2228.9)									

- ^{96}Mo -

G. S. band			γ-band			β_2-band			Octupole band		
[c] 0^+	0.0	(0.0)	2^+	1497.7	(1566.2)	0^+	1147.9	(1145.5)			
[c] 2^+	778.2	(748.1)	3^+	1973.4	(1917.6)				[c] 3^-	2233.5	(2264.3)
[c] 4^+	1628.2	(1564.0)									
6^+	2440.8	(2411.5)									

- ^{98}Mo -

G. S. band			γ-band			β_2-band			Octupole band		
[c] 0^+	0.0	(0.0)	2^+	1758.5	(1726.4)	0^+	734.8	(748.1)			
[c] 2^+	787.4	(667.8)	3^+	2104.7	(2022.5)	2^+	1432.3	(1511.2)	[c] 3^-	2017.5	(2030.9)
[c] 4^+	1510.0	(1487.3)									
6^+	2343.6	(2348.2)									

- ^{100}Mo -

G. S. band[†]			γ-band[†]			β_2-band[†]			Octupole band[†]		
[c] 0^+	0.0	(0.0)	2^+	1463.9	(1410.5)	0^+	695.1	(657.8)			
[c] 2^+	535.6	(491.2)	3^+	1607.4	(1609.2)	2^+	1063.8	(1230.8)	[c] 3^-	1908.3	(1908.7)
[c] 4^+	1136.1	(1131.0)	4^+	1771.5	(1797.9)	4^+	2103.2	(1839.7)			
6^+	1846.9	(2002.6)									

- ^{102}Ru -

G. S. band[†]			γ-band			β_2-band			Octupole band		
[c] 0^+	0.0	(0.0)	2^+	1103.2	(1145.1)	0^+	944.0	(963.8)			
[c] 2^+	475.1	(481.0)	3^+	1521.7	(1416.2)	2^+	1580.6	(1489.6)	[c] 3^-	2043.5	(2089.3)
[c] 4^+	1106.3	(1123.4)									
6^+	1873.2	(1863.3)									
8^+	2703.2	(2735.2)									

- ^{104}Pd -

table continued on next page

continued from previous page

G. S. band†			γ-band			β_2-band			Octupole band		
[c] 0^+	0.0	(0.0)	2^+	1341.7	(1376.1)	0^+	1333.6	(1278.9)			
[c] 2^+	555.8	(525.9)	3^+	1820.7	(1720.4)	2^+	1794.3	(1791.4)	[c] 3^-	2192.0	(2255.5)
[c] 4^+	1323.6	(1323.0)				4^+	2265.3	(2426.2)			
6^+	2249.5	(2246.5)									
8^+	3220.7	(3303.4)									

- ^{106}Pd -

G. S. band†			γ-band			β_2-band			Octupole band		
[c] 0^+	0.0	(0.0)	2^+	1128.0	(1158.5)	0^+	1133.8	(1087.7)			
[c] 2^+	511.9	(499.6)	3^+	1557.7	(1477.6)	2^+	1562.2	(1597.1)	[c] 3^-	2083.9	(2093.1)
[c] 4^+	1229.2	(1202.3)	4^+	1932.3	(1977.8)	4^+	2076.6	(2167.5)			
6^+	2076.3	(2039.3)									
8^+	2962.5	(3051.0)									

- ^{108}Pd -

G. S. band†			γ-band			β_2-band			Octupole band		
[c] 0^+	0.0	(0.0)	2^+	931.1	(953.3)	0^+	1052.8	(1008.2)			
[c] 2^+	433.9	(434.0)	3^+	1335.2	(1244.7)	2^+	1441.2	(1462.8)	[c] 3^-	2046.7	(2001.6)
[c] 4^+	1048.2	(1036.6)	4^+	1625.2	(1669.4)	4^+	1957.1	(1961.5)	5^-	2324.8	(2388.8)
6^+	1771.2	(1785.6)									
8^+	2548.4	(2499.8)									

- ^{110}Pd -

G. S. band†			γ-band			β_2-band			Octupole band		
[c] 0^+	0.0	(0.0)	2^+	813.6	(849.9)	0^+	946.7	(903.4)	1^-	2125.3	(1994.1)
[c] 2^+	373.8	(367.8)	3^+	1212.2	(1105.0)	2^+	1214.4	(1284.3)	[c] 3^-	2037.7	(2188.8)
[c] 4^+	920.8	(895.9)	4^+	1398.2	(1465.9)	4^+	1719.1	(1707.7)			
6^+	1574.0	(1548.1)									
8^+	2296.0	(2349.6)									

- ^{106}Cd -

G. S. band†			γ-band			β_2-band			Octupole band		
[c] 0^+	0.0	(0.0)	2^+	1716.5	(1761.9)	0^+	1795.2	(1737.6)			
[c] 2^+	632.6	(613.1)	3^+	2254.0	(2114.0)	2^+	2370.6	(2435.3)	[c] 3^-	2378.5	(2396.8)
4^+	1493.8	(1538.5)									
6^+	2491.7	(2545.2)									

- ^{108}Cd -

G. S. band†			γ-band			β_2-band			Octupole band		
[c] 0^+	0.0	(0.0)	2^+	1601.8	(1657.4)	0^+	1720.7	(1716.1)			
[c] 2^+	633.0	(620.2)	3^+	2145.9	(2045.5)	2^+	2365.8	(2368.6)	[c] 3^-	2202.2	(2231.8)
4^+	1508.5	(1553.3)	4^+	2738.9	(2644.1)						
6^+	2541.4	(2592.6)									

- ^{110}Cd -

G. S. band†			γ-band			β_2-band			Octupole band†		

table continued on next page

continued from previous page

[c] 0^+	0.0	(0.0)	2^+	1475.8	(1560.5)	0^+	1473.1	(1483.5)			
[c] 2^+	657.8	(653.9)	3^+	2162.8	(1945.2)				[c] 3^-	2078.9	(2073.7)
4^+	1542.5	(1547.2)									
6^+	2479.9	(2551.7)									

- ^{112}Cd -

G. S. band[†]			γ-band			β_2-band			Octupole band[†]		
[c] 0^+	0.0	(0.0)	2^+	1312.4	(1417.9)	0^+	1224.5	(1233.3)			
[c] 2^+	617.5	(615.7)	3^+	2064.6	(1745.2)				[c] 3^-	2005.3	(1996.9)
[c] 4^+	1415.6	(1404.7)									
6^+	2168.0	(2269.5)									

- ^{114}Cd -

G. S. band[†]			γ-band			β_2-band			Octupole band		
[c] 0^+	0.0	(0.0)	2^+	1209.7	(1303.4)	0^+	1134.5	(1140.9)			
[c] 2^+	558.5	(556.5)	3^+	1864.3	(1601.5)				[c] 3^-	1958.1	(1961.2)
4^+	1283.7	(1273.8)									
6^+	1990.3	(2068.5)									

- ^{116}Cd -

G. S. band[†]			γ-band			β_2-band			Octupole band		
[c] 0^+	0.0	(0.0)	2^+	1213.0	(1296.5)	0^+	1282.6	(1281.1)			
[c] 2^+	513.5	(501.8)	3^+	1915.8	(1632.9)				[c] 3^-	1921.5	(1922.7)
[c] 4^+	1219.4	(1233.1)									
6^+	2026.7	(2097.5)									

- ^{116}Sn -

G. S. band			γ-band			β_2-band			Octupole band		
[c] 0^+	0.0	(0.0)	2^+	2112.3	(2200.0)	0^+	1756.8	(1836.7)			
[c] 2^+	1293.6	(1299.7)	3^+	2996.3	(2767.5)				[c] 3^-	2266.2	(2266.5)
4^+	2390.9	(2492.6)									

- ^{118}Sn -

G. S. band			γ-band			β_2-band			Octupole band		
[c] 0^+	0.0	(0.0)	2^+	2043.0	(2035.8)	0^+	1758.0	(1807.7)			
[c] 2^+	1229.7	(1213.7)							[c] 3^-	2325.7	(2330.9)
4^+	2280.3	(2318.0)									

- ^{120}Sn -

G. S. band			γ-band			β_2-band			Octupole band		
[c] 0^+	0.0	(0.0)	2^+	2097.1	(2064.0)	0^+	1875.0	(1907.2)			
[c] 2^+	1171.3	(1128.2)							[c] 3^-	2399.3	(2396.1)
4^+	2194.5	(2284.0)									

- ^{122}Sn -

G. S. band			γ-band			β_2-band			Octupole band		
[c] 0^+	0.0	(0.0)	2^+	2153.5	(2124.6)	0^+	2088.0	(2034.7)			

table continued on next page

continued from previous page

[c]	2^+	1140.3	(1108.0)						[c]	3^-	2492.5 (2508.5)
	4^+	2141.7	(2261.2)								

- ^{124}Sn -

G. S. band			γ-band			β_2-band			Octupole band		
[c]	0^+	0.0 (0.0)	2^+	2129.6	(2100.0)	0^+	2129.3	(2067.0)			
[c]	2^+	1131.7 (1090.9)							[c]	3^-	2602.5 (2601.2)
	4^+	2101.7 (2253.9)									

- ^{122}Te -

G. S. band[†]			γ-band			β_2-band			Octupole band		
[c]	0^+	0.0 (0.0)	2^+	1257.0	(1337.5)	0^+	1357.4	(1359.4)			
[c]	2^+	564.1 (538.7)	3^+	1951.9	(1652.2)				[c]	3^-	2196.8 (2159.1)
	4^+	1181.2 (1286.4)									

- ^{124}Te -

G. S. band			γ-band			β_2-band			Octupole band		
[c]	0^+	0.0 (0.0)	2^+	1325.5	(1303.4)	0^+	1657.3	(1624.0)			
[c]	2^+	602.7 (566.0)							[c]	3^-	2293.7 (2280.0)
	4^+	1248.6 (1371.3)									

- ^{126}Te -

G. S. band			γ-band			β_2-band			Octupole band		
[c]	0^+	0.0 (0.0)	2^+	1420.2	(1474.0)	0^+	1873.4	(1859.1)			
[c]	2^+	666.4 (623.2)	3^+	2128.4	(1884.4)				[c]	3^-	2385.8 (2300.4)
	4^+	1361.4 (1531.0)									

- ^{128}Te -

G. S. band[†]			γ-band			β_2-band			Octupole band		
[c]	0^+	0.0 (0.0)	2^+	1520.0	(1541.8)	0^+	1978.8	(1950.8)			
[c]	2^+	743.2 (699.3)	3^+	2133.3	(1992.6)				[c]	3^-	2440.2 (2410.1)
	4^+	1497.0 (1670.1)									

- ^{130}Te -

G. S. band			γ-band			β_2-band			Octupole band		
[c]	0^+	0.0 (0.0)	2^+	1588.3	(1574.5)	0^+	1964.8	(1930.0)			
[c]	2^+	839.5 (789.8)	3^+	2138.6	(2062.6)				[c]	3^-	2527.1 (2500.9)
	4^+	1633.0 (1795.9)									

- ^{144}Nd -

G. S. band[†]			γ-band			β_2-band			Octupole band[†]		
[c]	0^+	0.0 (0.0)	2^+	1560.9	(1598.7)	0^+	2084.7	(1968.8)			
[c]	2^+	696.6 (594.1)	3^+	2179.0	(1978.2)				[c]	3^-	1510.9 (1435.3)
	4^+	1314.6 (1518.3)								5^-	2093.3 (2337.1)

- ^{150}Nd -

G. S. band[†]			γ-band[†]			β_2-band[†]			Octupole band[†]		

table continued on next page

continued from previous page

[c] 0^+	0.0	(0.0)	2^+	1062.0	(1110.1)	0^+	675.4	(690.4)	1^-	852.9	(828.0)
[c] 2^+	130.2	(129.4)	3^+	1200.6	(1183.8)	2^+	850.7	(837.4)	[c] 3^-	934.9	(947.6)
[c] 4^+	381.4	(388.8)	4^+	1353.4	(1281.8)	4^+	1137.8	(1133.6)	5^-	1129.0	(1151.6)
[c] 6^+	720.4	(729.2)				6^+	1541.2	(1521.8)			
[c] 8^+	1129.7	(1120.3)									
10^+	1599.0	(1544.6)									

- ^{148}Sm -

G. S. band[†]			γ-band			β_2-band			Octupole band[†]		
[c] 0^+	0.0	(0.0)	2^+	1454.1	(1521.4)	0^+	1424.5	(1258.1)			
[c] 2^+	550.3	(509.0)	3^+	1903.8	(1760.2)	2^+	1664.3	(1806.0)	[c] 3^-	1161.5	(1196.7)
[c] 4^+	1180.3	(1225.6)									
6^+	1905.9	(1980.1)									
8^+	2715.0	(2743.6)									
10^+	3398.1	(3524.2)									

- ^{150}Sm -

G. S. band[†]			γ-band			β_2-band			Octupole band[†]		
[c] 0^+	0.0	(0.0)	2^+	1193.7	(1272.9)	0^+	740.4	(707.0)	1^-	1165.6	(965.6)
[c] 2^+	333.9	(312.8)	3^+	1504.4	(1392.8)	2^+	1046.0	(1062.3)	[c] 3^-	1071.3	(1155.4)
[c] 4^+	773.2	(765.4)							5^-	1357.5	(1463.3)
[c] 6^+	1278.8	(1275.6)									
8^+	1836.9	(1798.5)									
10^+	2433.0	(2325.0)									

- ^{152}Sm -

G. S. band[†]			γ-band[†]			β_2-band[†]			Octupole band[†]		
[c] 0^+	0.0	(0.0)	2^+	1085.9	(1184.6)	0^+	684.7	(672.6)	1^-	963.4	(990.5)
[c] 2^+	121.8	(121.2)	3^+	1233.9	(1258.7)	2^+	810.5	(803.1)	[c] 3^-	1041.1	(1098.8)
[c] 4^+	366.5	(368.7)	4^+	1371.7	(1356.3)	4^+	1023.0	(1077.1)	5^-	1221.5	(1286.2)
[c] 6^+	706.9	(698.8)	5^+	1559.6	(1471.8)						
[c] 8^+	1125.3	(1083.3)	6^+	1728.2	(1612.4)						
10^+	1609.2	(1506.3)	7^+	1945.8	(1759.3)						

- ^{154}Sm -

G. S. band[†]			γ-band[†]			β_2-band[†]			Octupole band[†]		
[c] 0^+	0.0	(0.0)	2^+	1440.0	(1518.1)	0^+	1099.3	(1067.6)	1^-	921.4	(911.1)
[c] 2^+	82.0	(82.9)	3^+	1539.3	(1579.6)	2^+	1177.8	(1164.3)	[c] 3^-	1012.4	(1014.4)
[c] 4^+	266.8	(268.9)	4^+	1664.9	(1661.2)	4^+	1337.6	(1378.5)	5^-	1180.7	(1195.7)
[c] 6^+	543.7	(544.0)	5^+	1804.7	(1761.1)	6^+	1576.6	(1690.0)			
[c] 8^+	902.6	(893.1)	6^+	1946.2	(1881.4)	8^+	2138.8	(2078.0)			
10^+	1332.8	(1303.1)	7^+	2153.8	(2015.5)						

- ^{160}Gd -

G. S. band[†]			γ-band[†]			β_2-band[†]			Octupole band[†]		
[c] 0^+	0.0	(0.0)	2^+	988.4	(993.5)	0^+	1325.7	(1293.7)	1^-	1224.3	(1184.4)
[c] 2^+	75.3	(77.1)	3^+	1057.5	(1061.9)	2^+	1377.1	(1381.6)	[c] 3^-	1290.1	(1289.5)
[c] 4^+	248.5	(251.9)	4^+	1147.8	(1153.1)	4^+	1537.4	(1579.5)	5^-	1427.9	(1473.6)

table continued on next page

continued from previous page

[c] 6^+	514.8	(514.2)	5^+	1261.1	(1263.2)
[c] 8^+	867.9	(851.7)	6^+	1392.8	(1399.0)
10^+	1300.7	(1252.2)	7^+	1548.6	(1544.6)
			8^+	1717.0	(1725.9)

- ^{164}Dy -

G. S. band[†]			γ-band[†]			β_2-band			Octupole band[†]		
[c] 0^+	0.0	(0.0)	2^+	761.8	(754.6)	0^+	1655.4	(1522.7)			
[c] 2^+	73.4	(75.1)	3^+	828.2	(824.0)				[c] 3^-	1039.3	(1039.0)
[c] 4^+	242.2	(246.0)	4^+	916.0	(918.0)						
[c] 6^+	501.3	(503.4)	5^+	1024.6	(1029.4)						
[c] 8^+	843.7	(835.2)	6^+	1155.8	(1173.3)						
10^+	1261.3	(1229.4)	7^+	1302.6	(1318.4)						

- ^{166}Er -

G. S. band[†]			γ-band[†]			β_2-band[†]			Octupole band		
[c] 0^+	0.0	(0.0)	2^+	785.9	(785.9)	0^+	1459.9	(1430.5)			
[c] 2^+	80.6	(81.5)	3^+	859.4	(859.4)	2^+	1528.2	(1522.7)	[c] 3^-	1513.7	(1514.0)
[c] 4^+	265.0	(265.9)	4^+	956.2	(958.8)	4^+	1673.6	(1730.0)			
[c] 6^+	545.4	(541.2)	5^+	1075.3	(1076.1)						
[c] 8^+	911.2	(892.4)	6^+	1215.9	(1227.8)						
10^+	1349.6	(1305.3)	7^+	1376.0	(1379.2)						

- ^{168}Er -

G. S. band[†]			γ-band[†]			β_2-band[†]			Octupole band[†]		
[c] 0^+	0.0	(0.0)	2^+	821.2	(828.3)	0^+	1217.2	(1183.2)	1^-	1358.9	(1323.7)
[c] 2^+	79.8	(83.8)	3^+	895.8	(900.1)	2^+	1276.3	(1280.2)	[c] 3^-	1431.5	(1432.3)
[c] 4^+	264.1	(271.8)	4^+	994.7	(996.8)	4^+	1411.1	(1495.5)	5^-	1574.1	(1621.6)
[c] 6^+	548.7	(548.7)	5^+	1117.6	(1111.0)						
[c] 8^+	928.3	(897.3)	6^+	1263.9	(1256.7)						
10^+	1396.8	(1301.9)	7^+	1432.9	(1403.5)						
			8^+	1624.5	(1602.5)						

- ^{174}Yb -

G. S. band[†]			γ-band[†]			β_2-band[†]			Octupole band[†]		
[c] 0^+	0.0	(0.0)	2^+	1634.0	(1645.4)	0^+	1487.1	(1474.0)			
[c] 2^+	76.5	(77.0)	3^+	1709.4	(1712.2)	2^+	1561.0	(1558.4)	[c] 3^-	1382.0	(1383.9)
[c] 4^+	253.1	(254.2)	4^+	1805.4	(1800.7)	4^+	1715.4	(1751.9)	5^-	1572.1	(1569.4)
[c] 6^+	526.0	(525.8)	5^+	1926.0	(1910.3)						
[c] 8^+	889.9	(884.3)									
10^+	1336.0	(1321.6)									

- ^{176}Yb -

G. S. band[†]			γ-band[†]			β_2-band[†]			Octupole band[†]		
[c] 0^+	0.0	(0.0)	2^+	1260.9	(1267.5)	0^+	1139.0	(1123.3)	1^-	1088.2	(1091.7)
[c] 2^+	82.1	(85.5)	3^+	1336.4	(1336.7)	2^+	1199.6	(1223.1)	[c] 3^-	1193.3	(1203.6)
[c] 4^+	271.7	(277.3)	4^+	1435.4	(1428.5)				5^-	1409.6	(1399.6)
[c] 6^+	564.7	(561.1)	5^+	1558.3	(1540.0)						
[c] 8^+	954.0	(921.2)									

table continued on next page

continued from previous page

10^+	1431.0	(1343.6)									

- ^{178}Hf -

G. S. band†			γ-band†			β_2-band†			Octupole band		
[c] 0^+	0.0	(0.0)	2^+	1174.6	(1197.1)	0^+	1199.4	(1166.0)			
[c] 2^+	93.2	(95.8)	3^+	1268.5	(1274.1)	2^+	1276.7	(1275.5)	[c] 3^-	1322.5	(1334.7)
[c] 4^+	306.6	(310.5)	4^+	1384.5	(1376.5)	4^+	1450.4	(1519.2)	5^-	1512.6	(1530.4)
[c] 6^+	632.2	(627.1)	5^+	1533.2	(1500.2)						
8^+	1058.6	(1027.2)									
10^+	1571.0	(1494.3)									

- ^{180}Hf -

G. S. band†			γ-band†			β_2-band†			Octupole band		
[c] 0^+	0.0	(0.0)	2^+	1199.7	(1216.9)	0^+	1101.9	(1091.7)			
[c] 2^+	93.3	(96.0)	3^+	1291.0	(1296.3)	2^+	1183.3	(1197.9)	[c] 3^-	1354.1	(1354.0)
[c] 4^+	308.6	(311.3)	4^+	1409.2	(1401.4)	4^+	1369.5	(1437.5)			
[c] 6^+	640.9	(629.1)	5^+	1556.8	(1528.8)						
8^+	1083.9	(1031.5)									

- ^{182}W -

G. S. band†			γ-band†			β_2-band†			Octupole band†		
[c] 0^+	0.0	(0.0)	2^+	1221.4	(1257.3)	0^+	1135.8	(1143.3)			
[c] 2^+	100.1	(104.8)	3^+	1331.1	(1338.4)	2^+	1257.4	(1263.9)	[c] 3^-	1373.8	(1392.4)
[c] 4^+	329.4	(337.8)	4^+	1442.8	(1446.4)	4^+	1510.2	(1529.9)	5^-	1621.3	(1607.5)
[c] 6^+	680.5	(677.8)	5^+	1623.5	(1576.3)						
8^+	1144.4	(1102.8)	6^+	1769.5	(1736.2)						
10^+	1711.9	(1594.4)									

- ^{184}W -

G. S. band†			γ-band†			β_2-band†			Octupole band†		
[c] 0^+	0.0	(0.0)	2^+	903.3	(913.4)	0^+	1002.5	(994.6)			
[c] 2^+	111.2	(117.8)	3^+	1006.0	(1003.3)	2^+	1121.4	(1129.2)	[c] 3^-	1221.3	(1287.0)
[c] 4^+	364.1	(372.6)	4^+	1133.8	(1124.2)	4^+	1360.4	(1421.2)	5^-	1492.0	(1512.4)
[c] 6^+	748.3	(730.4)									
8^+	1252.3	(1160.3)									
10^+	1861.3	(1640.2)									

- ^{192}Os -

G. S. band†			γ-band†			β_2-band†			Octupole band		
[c] 0^+	0.0	(0.0)	2^+	489.1	(487.8)	0^+	956.5	(962.8)			
[c] 2^+	205.8	(203.1)	3^+	690.4	(669.7)	2^+	1127.5	(1133.5)	[c] 3^-	1341.2	(1359.6)
[c] 4^+	580.3	(586.6)	4^+	909.6	(970.4)						
[c] 6^+	1089.2	(1053.7)	5^+	1143.5	(1164.2)						
8^+	1708.4	(1587.4)									

- ^{194}Pt -

G. S. band†			γ-band†			β_2-band			Octupole band		
[c] 0^+	0.0	(0.0)	2^+	622.0	(623.9)	0^+	1267.2	(1253.1)			

table continued on next page

continued from previous page

[c] 2^+	328.5	(306.8)	3^+	922.8	(877.7)				[c] 3^-	1432.5	(1439.2)
[c] 4^+	811.3	(820.2)	4^+	1229.5	(1379.6)						
6^+	1411.8	(1338.5)									
8^+	2099.5	(2026.8)									

- ^{232}Th -

G. S. band[†]			γ-band[†]			β_2-band[†]			Octupole band[†]		
[c] 0^+	0.0	(0.0)	2^+	785.2	(796.9)	0^+	730.6	(706.3)	1^-	714.4	(713.4)
[c] 2^+	49.4	(50.1)	3^+	829.6	(836.4)	2^+	774.1	(763.5)	[c] 3^-	774.4	(779.4)
[c] 4^+	162.1	(163.5)	4^+	890.1	(889.0)	4^+	873.0	(891.7)	5^-	883.8	(895.6)
[c] 6^+	333.3	(332.8)	5^+	960.2	(953.3)	6^+	1023.3	(1080.9)			
[c] 8^+	556.9	(549.7)	6^+	1050.9	(1031.3)						
10^+	826.8	(806.4)									
12^+	1137.1	(1095.7)									

- ^{238}U -

G. S. band[†]			γ-band[†]			β_2-band[†]			Octupole band[†]		
[c] 0^+	0.0	(0.0)	2^+	1060.3	(1073.3)	0^+	997.2	(988.1)	1^-	680.1	(684.1)
[c] 2^+	44.9	(44.8)	3^+	1105.7	(1111.3)	2^+	1037.3	(1037.7)	[c] 3^-	731.9	(749.8)
[c] 4^+	148.4	(147.9)	4^+	1163.0	(1161.9)	4^+	1130.8	(1151.3)	5^-	826.6	(866.6)
[c] 6^+	307.2	(306.1)	5^+	1232.0	(1224.4)	6^+	1269.2	(1324.7)			
[c] 8^+	518.1	(515.0)	6^+	1311.0	(1299.8)						
10^+	775.9	(769.8)									
12^+	1076.7	(1065.6)									

[†] The band was determined by reference to the latest versions of Nuclear Data Sheets.

[c] The level was employed in the SRM-CC computation.

3.1.2 Limitations on the Level Structure Analysis

It was difficult to carry out the level structure analysis for some of the transitional nuclei. It was just because most of these isotopes exhibited an unusually level structure. In general, the level energy ratio $E(4_1^+)/E(2_1^+)$ is almost equal to 2.0 for the typical vibrational nuclei, and the value varies from ~ 2.0 to ~ 3.3 for the rotational-vibrational nuclei. However, for example, the major Zr even-even isotopes are influenced by a neutron magic shell, and their values of $E(4_1^+)/E(2_1^+)$ result in ~ 1.5. This phenomenon is beyond the SRM rotational-vibrational theory, so it is impossible to reproduce those level allocations by the present version of SRM. According to those facts, we did not carry out the SRM analysis for the nuclei which apparently exhibit $E(4_1^+)/E(2_1^+) \lesssim 2.0$ even if the measured proton scattering data were abundant.

There existed another problem in the assumption of the level structure. It was difficult to identify the members of the γ-vibrational band ($\tau = 2$, $n_\gamma = 1$, $n_{\beta_2} = 0$, $n_{\beta_3} = 0$) for most of nuclei. Actually, the band head positioned at relatively high excitation energy region where we found out a lot of the

candidate levels. So we did not consider this band purposely in the level structure analysis. Since the level data of this band were essential to deduce the softness of γ-vibration, the value of the parameter μ_{γ_0} were not obtained in this work. Note that it gave no effects on other parameter values.

3.2 Coupled-channels Optical Model Analysis

3.2.1 Purpose of the Model Analysis

It is important to obtain a reliable value of the equilibrium G.S. deformation parameter in order to determine the whole parameter set. However, it was impossible to deduce certain values of β_{20} and β_4 just by the SRM level structure analysis, since these equilibrium deformation parameters appear only as a perturbation in the level energies. Thus, we tried to derive the values from the experimental data of particle inelastic scattering cross sections by the optical model analysis. We employed the coupled-channels (CC) method which adopted the coupling strengths calculated by the SRM Hamiltonian. The method will be called "SRM-CC" thereafter in this paper. The value of β_{20} was determined so as to describe the measured data of the first 2_1^+ excitation. Also, the first 2_1^+ and 4_1^+ data were simultaneously analyzed in order to obtain the value of β_{20} and β_4 if the hexadecapole deformation was additionally assumed. Since the value of ϵ_0 $(= \beta_{30}/\beta_{20})$ was somewhat sensitive to the level calculations, it was deduced by the SRM level structure analysis while the measured cross sections were refered in the estimation of its initial guess. A CC optical model code OPTMAN[2] was adopted for those computations. The code partially includes the main part of the SHEMMAN code, and it enables us to carry out the SRM-CC calculations.

In this work, we restricted our efforts to the analyses for inelastic proton scattering cross sections due to the reasons as follows.

- Relatively many experimental works have been devoted to obtained the differential cross sections of protons, and a lot of their numerical values were available from an experimental nuclear reaction database EXFOR[§].
- A CC optical model potential was empirically formulated for nucleons up to 200 MeV over a wide (medium-heavy) mass range by our recent study[13]. Though this potential had been obtained based on the rigid-rotator model, it was expected to be almost equivalent to the potential which should be used in the SRM-CC calculations above $\sim$ 10 MeV as mentioned in the next subsection.
- Proton (charged-particle) data are generally measured with small errors and fine resolutions compared to the neutron data. Thus, it was expected that the deformation parameters would be determined more precisely.

[§]It is available on the Internet (e.g., http://www.nea.fr)

- Of course, it was possible to carry out the SRM-CC analyses by using the neutron scattering data. The measured data are abundant for a limited number of nuclei compared to proton data, however, most of them are obtained in a lower energy range ($\lesssim$ 20 MeV) where the statistical process is not negligible. Namely, the choice of statistical model parameters may somewhat affect the deformation parameters to be determined.

Note that this approach could be applied only to the nuclei of which inelastic scattering experimental data were available. That is the reason why we did SRM and SRM-CC analyses for ^{56,58}Fe, ^{60,62,64}Ni, $^{64-70}$Zn, $^{70-76}$Ge, $^{74-82}$Se, ^{86}Sr, ^{96,98,100}Mo, ^{102}Ru, $^{104-110}$Pd, $^{106-116}$Cd, $^{116-124}$Sn, $^{122-130}$Te, ^{144,150}Nd, $^{148-154}$Sm, ^{160}Gd, ^{166}Dy, ^{166,168}Er, ^{174,176}Yb, ^{178,180}Hf, ^{182,184}W, ^{192}Os, ^{194}Pt, ^{232}Th and ^{238}U. The employed measured (p, p') data are listed in **Table 2** for each nucleus. If experimental cross sections were available at more than two incident energies, the value of β_{20} and β_4 were determined to give an overall description of those data.

Table 2: Experimental data for inelastic scattering differential cross sections of protons which were employed in the SRM-CC analyses

	E_p (MeV)	Reference	G.S. band	β_3-band
^{56}Fe	17.2, 20.4, 24.6	Hall *et al.*[14]	2_1^+	
	49.35	Mani [15]	2_1^+, (4_1^+)	(3_1^-)
	65.0	Takamatsu *et al.*[16]	2_1^+	
	65.0	Leo *et al.*[17]	2_1^+, (4_1^+)	(3_1^-)
^{58}Fe	49.35	Mani [18]	2_1^+, (4_1^+)	(3_1^-)
^{60}Ni	20.4, 24.6	Hall *et al.*[14]	2_1^+	(3_1^-)
	40.0	Lingappa *et al.*[19]	2_1^+, (4_1^+)	(3_1^-)
	178.0	Ingemarsson *et al.*[20]	2_1^+, (4_1^+)	(3_1^-)
^{62}Ni	20.4, 24.6	Hall *et al.*[14]	2_1^+	(3_1^-)
^{64}Ni	20.4	Hall *et al.*[21]	2_1^+	(3_1^-)
^{64}Zn	20.4	Moonen *et al.*[22]	2_1^+, (4_1^+)	(3_1^-)
	30.5	Tait *et al.*[23]	2_1^+	(3_1^-)
	49.1	Calderbank *et al.*[24]	2_1^+, (4_1^+)	(3_1^-)
^{66}Zn	20.4	Moonen *et al.*[22]	2_1^+, (4_1^+)	(3_1^-)
	30.5	Tait *et al.*[23]	2_1^+	(3_1^-)
	49.1	Calderbank *et al.*[24]	2_1^+, (4_1^+)	(3_1^-)
	55.1	Yagi *et al.*[25]	2_1^+	(3_1^-)
^{68}Zn	20.4	Moonen *et al.*[22]	2_1^+, (4_1^+)	(3_1^-)
	30.5	Tait *et al.*[23]	2_1^+	(3_1^-)
	49.1	Calderbank *et al.*[24]	2_1^+	(3_1^-)
^{70}Zn	20.4	Moonen *et al.*[22]	2_1^+	(3_1^-)
	49.1	Calderbank *et al.*[24]	2_1^+	(3_1^-)
$^{70-76}$Ge	22.3	Moonen *et al.*[26]	2_1^+, (4_1^+)	(3_1^-)
$^{76-80}$Se	22.3	Moonen *et al.*[26]	2_1^+, (4_1^+)	(3_1^-)
	16.0	Delaroche *et al.*[27]	2_1^+, (4_1^+)	(3_1^-)
^{82}Se	16.0	Delaroche *et al.*[27]	2_1^+	(3_1^-)
$^{74-82}$Se	64.8	Ogino [28]	2_1^+, (4_1^+)	(3_1^-)

table continued on next page

	E_p (MeV)	Reference	G.S. band	β_3-band
^{86}Sr	20.4	Hall *et al.*[21]	2_1^+	(3_1^-)
^{96}Mo	12.5	Burger *et al.*[29]	2_1^+, (4_1^+)	(3_1^-)
	15.0	Lutz *et al.*[30]	2_1^+, (4_1^+)	(3_1^-)
	25.6	Fretwurst *et al.*[31]	2_1^+, (4_1^+)	(3_1^-)
	30.5	Tait *et al.*[23]	2_1^+	
^{98}Mo	12.5	Burger *et al.*[29]	2_1^+, (4_1^+)	
	15.0	Lutz *et al.*[30]	2_1^+, (4_1^+)	
	22.3	Cereda *et al.*[32]	2_1^+	
^{100}Mo	15.0	Lutz *et al.*[30]	2_1^+, (4_1^+)	(3_1^-)
	22.3	Cereda *et al.*[32]	2_1^+	
	25.6	Fretwurst *et al.*[31]	2_1^+, (4_1^+)	(3_1^-)
	51.0	Pignanelli *et al.*[33]	2_1^+, (4_1^+)	(3_1^-)
^{102}Ru	22.3	Cereda *et al.*[32]	2_1^+	(3_1^-)
$^{104-110}$Pd	22.0	Aoki *et al.*[34]	2_1^+	(3_1^-)
^{104}Pd	10.3	Cereda *et al.*[32]	2_1^+	
	12.1, 15.0, 17.3, 30.2, 35.4		2_1^+	(3_1^-)
	22.3		2_1^+, (4_1^+)	(3_1^-)
^{106}Pd	22.3	Cereda *et al.*[32]	2_1^+, (4_1^+)	(3_1^-)
	51.9	Koike *et al.*[35]	2_1^+, (4_1^+)	(3_1^-)
^{108}Pd	22.3	Cereda *et al.*[32]	2_1^+	(3_1^-)
	51.9	Koike *et al.*[35]	2_1^+	(3_1^-)
^{110}Pd	22.3	Cereda *et al.*[32]	2_1^+, (4_1^+)	(3_1^-)
	51.9	Koike *et al.*[35]	2_1^+, (4_1^+)	(3_1^-)
^{106}Cd	22.3	Cereda *et al.*[32]	2_1^+	(3_1^-)
	22.3	Petit *et al.*[36]	2_1^+, (4_1^+)	(3_1^-)
^{108}Cd	22.3	Petit *et al.*[36]	2_1^+, (4_1^+)	
^{110}Cd	20.4	Hall *et al.*[21]	2_1^+	(3_1^-)
	22.3	Cereda *et al.*[32]	2_1^+	(3_1^-)
	22.3	Petit *et al.*[36]	2_1^+, (4_1^+)	(3_1^-)
^{112}Cd	20.4	Hall *et al.*[21]	2_1^+	(3_1^-)
	22.3	Cereda *et al.*[32]	2_1^+	(3_1^-)
	22.3	Petit *et al.*[36]	2_1^+, (4_1^+)	(3_1^-)
	51.0	Pignanelli *et al.*[33]	2_1^+, (4_1^+)	(3_1^-)
^{114}Cd	20.4	Hall *et al.*[21]	2_1^+	(3_1^-)
	22.3	Petit *et al.*[36]	2_1^+, (4_1^+)	(3_1^-)
^{116}Cd	22.3	Cereda *et al.*[32]	2_1^+	(3_1^-)
	22.3	Petit *et al.*[36]	2_1^+	(3_1^-)
$^{116-124}$Sn	20.4	Hall *et al.*[21]	2_1^+	(3_1^-)
^{120}Sn	24.6	Hall *et al.*[21]	2_1^+	(3_1^-)
	103.5	Kailas *et al.*[37]	2_1^+, (4_1^+)	(3_1^-)
^{144}Nd	35.0	Cottle *et al.*[38]	2_1^+, (4_1^+)	(3_1^-)
^{150}Nd	30.7	Pignanelli *et al.*[39]		3_1^-
$^{148-154}$Sm	16.0	Kruse *et al.*[40]	2_1^+	
^{148}Sm	66.5	Guterman *et al.*[41]	2_1^+	
^{152}Sm	65.0	Ichihara *et al.*[42]	2_1^+, 4_1^+, (6_1^+)	(3_1^-)
^{154}Sm	35.0	King *et al.*[43]	2_1^+, 4_1^+, (6_1^+)	
	65.0	Ichihara *et al.*[42]	2_1^+, 4_1^+, (6_1^+)	

table continued on next page

	E_p (MeV)	Reference	G.S. band	β_3-band
	66.5	Guterman *et al.*[41]	2_1^+, 4_1^+, (6_1^+)	
^{160}Gd	65.0	Ichihara *et al.*[42]	2_1^+, 4_1^+, (6_1^+)	(3_1^-)
^{164}Dy	65.0	Ichihara *et al.*[42]	2_1^+, 4_1^+, (6_1^+)	
^{166,168}Er	65.0	Ichihara *et al.*[44, 42]	2_1^+, 4_1^+, (6_1^+)	
^{174}Yb	16.0	Kruse *et al.*[40]	2_1^+	
	65.0	Ichihara *et al.*[44, 42]	2_1^+, 4_1^+, (6_1^+)	
^{176}Yb	30.0	Kamigaito *et al.*[45]	2_1^+, 4_1^+	
	65.0	Ichihara *et al.*[44, 42]	2_1^+, 4_1^+, (6_1^+)	
^{178,180}Hf	65.0	Ogawa *et al.*[46]	2_1^+, 4_1^+, (6_1^+)	
^{180}Hf	98.4	Perrino *et al.*[47]	2_1^+, 4_1^+, (6_1^+)	
^{182,184}W	65.0	Ogawa *et al.*[46, 42]	2_1^+, 4_1^+, (6_1^+)	
^{192}Os	16.0	Kruse *et al.*[40]	2_1^+	
	65.0	Ichihara *et al.*[42]	2_1^+, 4_1^+	
	134.5	Baker *et al.*[48]	2_1^+, 4_1^+	
^{194}Pt	16.0	Kruse *et al.*[40]	2_1^+	
	135.0	Sethi *et al.*[49]	2_1^+, 4_1^+	
^{232}Th, ^{238}U	20.0, 26.0	Hansen *et al.*[50]	2_1^+, 4_1^+	
	35.0	King *et al.*[51]	2_1^+, 4_1^+, (6_1^+)	
	65.0	Ichihara *et al.*[52]	2_1^+, 4_1^+, (6_1^+)	

· The parenthetic level's cross section data were not used in determining values of β_{20} and β_4.

· As for ^{150}Nd, the value of β_{20} was exceptionally determined in an analysis for the inelastic scattering cross sections from 3_1^-. Also, the value of β_4 was taken from that of ^{152}Sm.

3.2.2 Optical Model Potential

The optical potential is required for the SRM-CC computations. We should give an appropriate potential because it also determines cross sections to be calculated, thereby, the deformation parameters to be estimated. It might be a natural approach for us to adjust the optical potential parameters together with the deformation parameters for each nucleus. However, the optical potential varies with the target nucleus and the projectile type in general. Also, it strongly depends on the collision energy especially below 100 MeV. Furthermore, the optical potential is described with various parameters such as the potential radius, the surface diffuseness and the energy-dependent potential depth parameters involving the real, imaginary, volume, surface and spin-orbit terms. A reliable parameter set should be derived not only from the measured data of the particle scattering cross section but also from the total-reaction cross section and the analyzing power.

It was expected to be a preferable approach for us to adopt a global optical potential of protons which covers wide nuclear mass and energy ranges. Though a lot of global potentials had been proposed for nucleons until now, most of them could be applied in narrow nuclear-mass and energy regions. Moreover, they assumed the spherical nuclear-shape with a single-channel calculation, while the nucleus usually has collective nature where the CC method should gave more successful results. For those reasons, we

employed a systematic CC optical model potential formulated by us. Since it was already reported in Ref.[13], we just pick up its main features and advantages as follows.

- It is a nucleon potential which includes isospin dependent effects by introducing the symmetric and the Coulomb terms. The potential parameters were obtained by a simultaneous analysis of incident neutron and proton data. Thus this potential includes the experimental findings of neutron total and elastic-scattering cross sections as well as those of protons.

- This potential covers wide nuclear mass and energy ranges : $50 \lesssim A \lesssim 250$ ($26 \lesssim Z \lesssim 92$) and 1 keV to 200 MeV for collision energy. It allows us to do optical model calculations for the medium-heavy nuclei below proton energy of 200 MeV.

- Though the optical potential had been determined with the spherical model in general, our potential was deduced by using the CC method assuming the rigid nuclear-deformation and its rotation (RRM-CC) with standard coupling schemes. The use of RRM-CC potential in the SRM-CC calculation is reasonable since we did the proton scattering analysis at comparably high energies ($\gtrsim 10$ MeV) where the collective contributions progressively weaken. In this sense, the use of spherical potential might be also acceptable. However, we adopted the CC potential in order to obtain more realistic results at around several tens of MeV for the typical deformed nuclei as well as for the other nuclei. For a complete analysis in terms of SRM-CC, however, we admit that we have to search for the potential parameters, which will be a subject of our feature work.

As examples, **Fig. 1** shows the calculated differential cross sections of elastically scattered 65 MeV protons for medium and heavy nuclides such as ^{56}Fe, ^{100}Mo, ^{152}Sm, ^{184}W and ^{232}Th. The computations were done by SRM-CC with the obtained Hamiltonian parameters described later. The calculated results reproduce not only the experimental data of 65 MeV protons[17, 53, 46, 42, 52] but also the measurements over a wide energy range below 200 MeV.

3.2.3 Coupled Levels

The adopted coupled-levels are marked with "c" in Table 1 for each nucleus. We just coupled major levels of $\tau = 1$ in the present analyses. These levels corresponded to the members of the G.S. and octupole bands which were assigned as $\tau = 1$, $n_\gamma = 0$, $n_{\beta_2} = 0$ and $n_{\beta_3} = 0$. They were enough to obtain the value of the deformation parameter β_{20} (and β_4 for typical deformed nuclei) uniquely. The weakly coupled levels, i.e., the γ- and the β_2-vibrational states were purposely excluded from the CC calculations due to the reasons mentioned later.

The first 2^+ state is known to show the strongest collectivity among the low-lying levels in general. The succeeding 4_1^+, 6_1^+, $\cdots$ levels are also relatively strong if the nucleus has rotational-vibrational or rotational property. Accordingly, we always adopted 0_1^+ and 2_1^+ for the SRM-CC computation. Though we did not provide clear criteria for the adoption of the additional levels 4_1^+, 6_1^+, $\cdots$, the value of

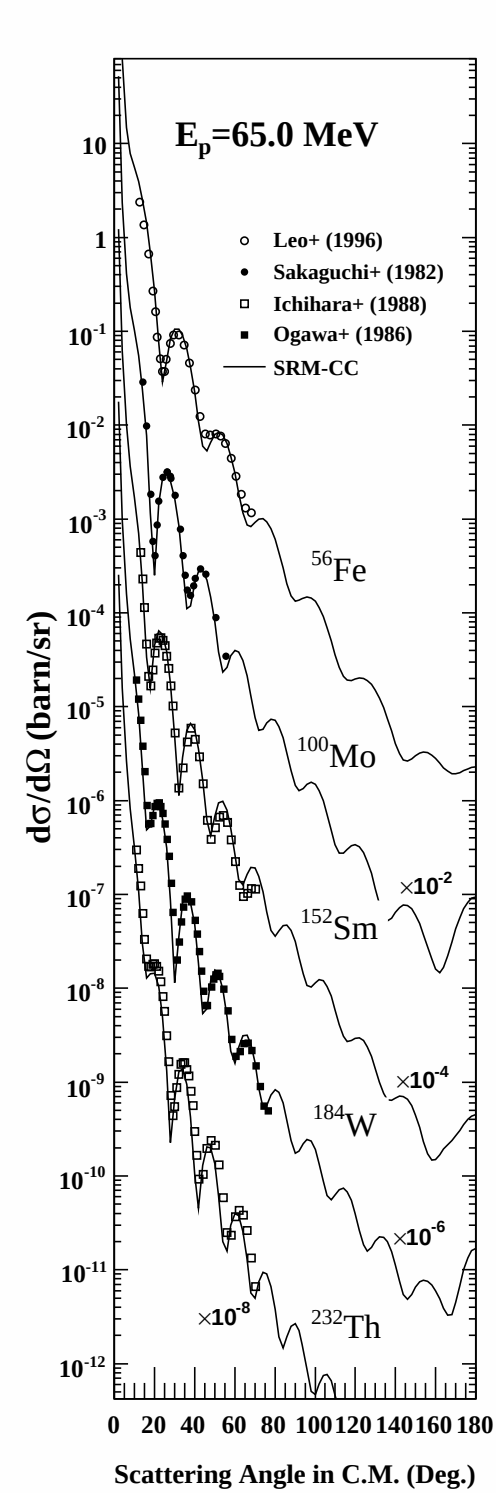

Fig. 1: Calculated elastic scattering differential cross sections of 65 MeV protons which are compared with the experimental data[17, 53, 46, 42, 52] for ^{56}Fe, ^{100}Mo, ^{152}Sm, ^{184}W and ^{232}Th. The computations were done by SRM-CC with deduced Hamiltonian parameters.

$E(4_1^+)/E(2_1^+)$ was an useful guide for this judgement. For examples, the levels 0_1^+, 2_1^+, (4_1^+) were coupled for the vibrational nuclides which exhibited $E(4_1^+)/E(2_1^+) \sim 2.0$. Meanwhile, the levels 0_1^+, 2_1^+, 4_1^+, 6_1^+, (8_1^+ and 10_1^+) were employed for the rotational-vibrational and rotational isotopes which exhibited $E(4_1^+)/E(2_1^+) \sim 3.0$. We always coupled the member of the octupole band 3_1^- together with the levels of G.S. band. The coupling of this level did not affect significantly the calculated particle scattering cross sections from 2_1^+ and 4_1^+ states, thereby, the value of β_{20} and β_4 to be determined, though it tends to show relatively strong collectivity for the vibrational and the rotational-vibrational nuclei in general. However, since the measured inelastic scattering cross sections from 3_1^- state were available for many nuclides, we adopted 3_1^- in order to investigate the validity of the octupole SRM parameters on the cross sections.

As mentioned in 1-3.1.2, the value of the softness of the γ-vibration μ_{γ_0} was not determined in the present analyses for all nuclei¶. Since the fact meant the coupling strengths could not be calculated for the members of the γ-band, we were enforced to exclude $\tau = 2$ levels from the coupling level scheme. It should be noted that the couplings of those levels hardly brought influences on the cross section of (p, p') from the 2_1^+ and 3_1^- states owing to their weak relative collectivities if we gave a reasonable value of μ_{γ_0}. Besides, the present CC calculations with consideration of 0_2^+ coupling were sometimes apt to badly predict the available experimental data of the differential cross sections of (p, p') from this level in the amplitude and/or the angular distribution. We must admit it could be due to the assumed band structures and/or an imperfection of the model itself which resulted in an insufficient description of the β_2-vibrational ($n_{\beta_2} = 1$) properties. However, the couplings of the $n_{\beta_2} = 1$ levels affected the cross section of (p, p') from the 2_1^+ and 3_1^- states just by negligible amount owing to its weak collectivity predicted. Though the values of deformation parameters were almost independent of whether the levels were coupled or not, we excluded the members of the β_2-vibrational band from the CC computations.

3.3 Parameter Searches

Since many SRM parameters had to be determined simultaneously for each nucleus using limited experimental data, their values were deduced with a combination of an automatic and the manual searches to give an overall description of experimental level and inelastic scattering proton data. The searches were based on our empirical insights which were mostly devoted to giving an initial Hamiltonian parameter set. For an example in the level structure analysis, we just assumed the quadrupole properties in the model as a first step. Then a tentative quadrupole parameter set was estimated. Next, temporary octupole parameters were searched for. In this step, both quadrupole and octupole properties were considered fixing the quadrupole parameter values. For typical deformed nuclei, the tentative hexadecapole parameters were also determined additionally. Thirdly, the quadrupole, octupole (and hexadecapole) parameters were determined almost simultaneously using the values obtained in the preceding two steps

¶If the inelastic scattering cross sections from these states are measured, as a way, the value of μ_{γ_0} can be determined so as to reproduce the experimental data.

as the initial guesses. The final results were obtained by more than 20 times iterations of the computer exercise for those three processes. The SRM-CC results sometimes could not reproduce experimental angular distribution of (p, p') from 2_1^+ (and 4_1^+) around a backward angle. In such cases, we determined the values of the deformation parameters to describe the measured data at a forward region ($\theta_{\mathrm{C.M.}} \lesssim 40^\circ$), because the cross sections were not so sensitive to slight differences of optical model potential in such an angular range.

Typical examples of the calculated and the experimental levels are illustrated in **Figs. 2-7** together with those of (p,p') differential cross sections. We could well describe the low-lying collective level structure of the typical vibrational nuclei such as ^{64}Ni and ^{100}Mo, the rotational-vibrational ones such as ^{82}Se and ^{110}Pd, and the rotational ones such as ^{152}Sm and ^{232}Th. The calculated level energies are given in parentheses in Table 1 for all nuclei of our interests. Also, SRM-CC reproduced the measured (p,p') differential cross sections from excitations of 2_1^+ and 4_1^+ states if we gave appropriate values of β_{20} and β_4. It should be noted that the measured 3_1^- cross sections are described fairly well. The worst result was obtained for ^{110}Pd where the calculated result seems to disagree with the experimental data in phase by 10°. As for ^{232}Th and some other deformed nuclei, the present results reproduced the measured cross sections from excitations of 6_1^+.

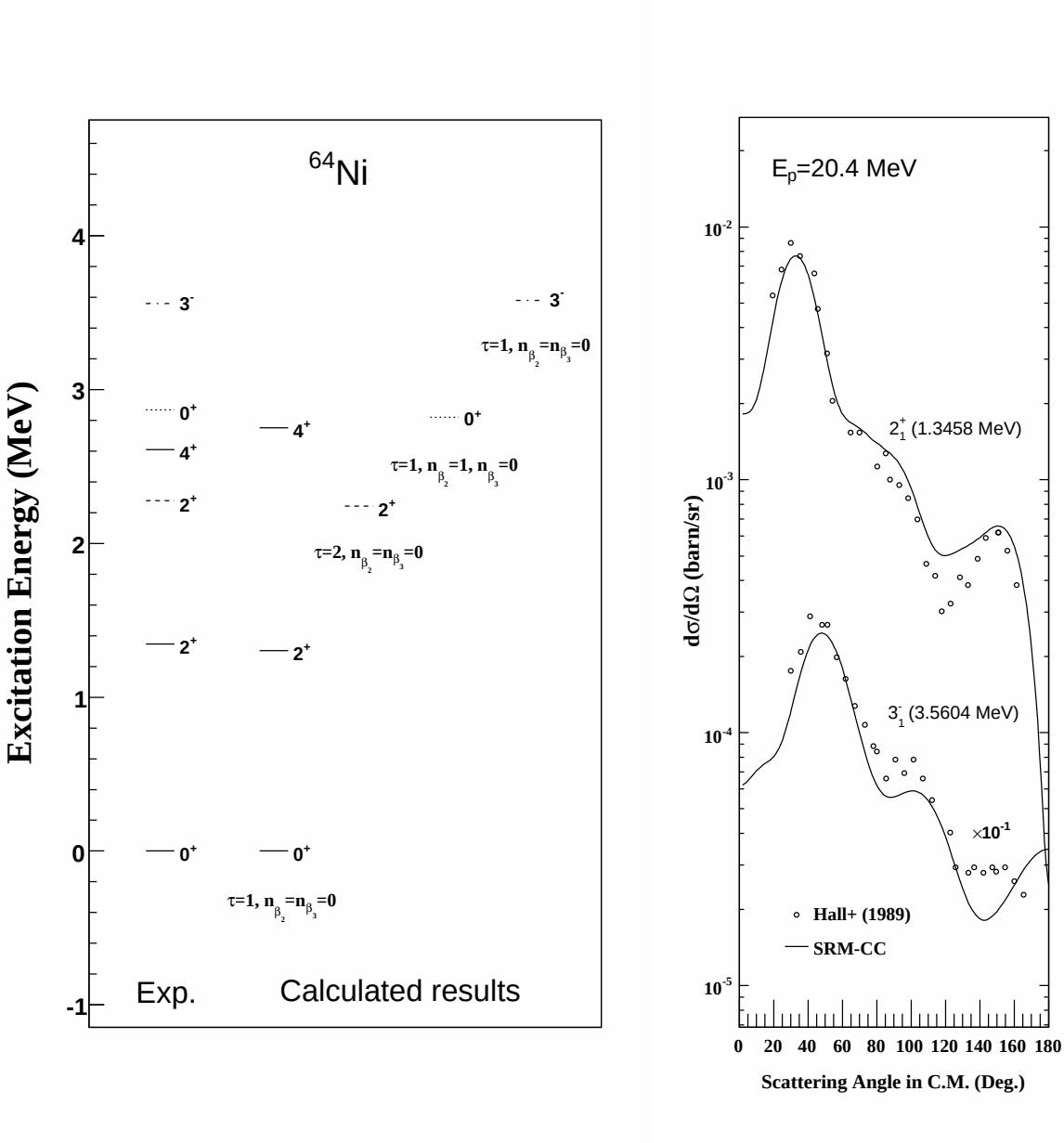

Fig. 2: The SRM(-CC) calculations obtained with the present Hamiltonian parameters which are compared to the experimental data for ^{64}Ni: The SRM low-lying level structure together with the experimental one (left) and the SRM-CC differential cross sections of inelastically-scattered protons at 20.4 MeV together with measured ones[21] (right)

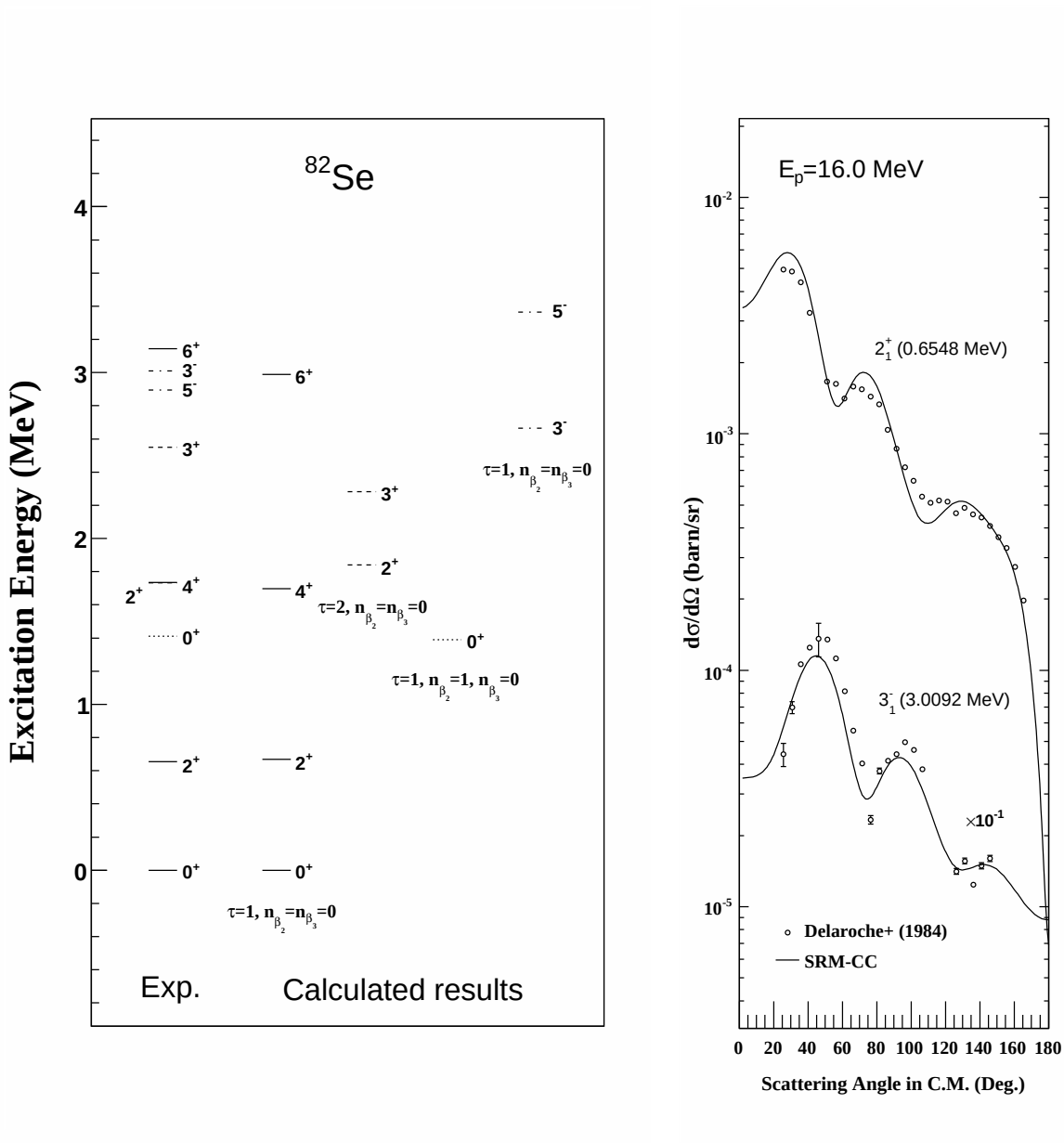

Fig. 3: The SRM(-CC) calculations obtained with the present Hamiltonian parameters which are compared to the experimental data for ^{82}Se: The SRM low-lying level structure together with the experimental one (left) and the SRM-CC differential cross sections of inelastically-scattered protons at 16.0 MeV together with measured ones[27] (right)

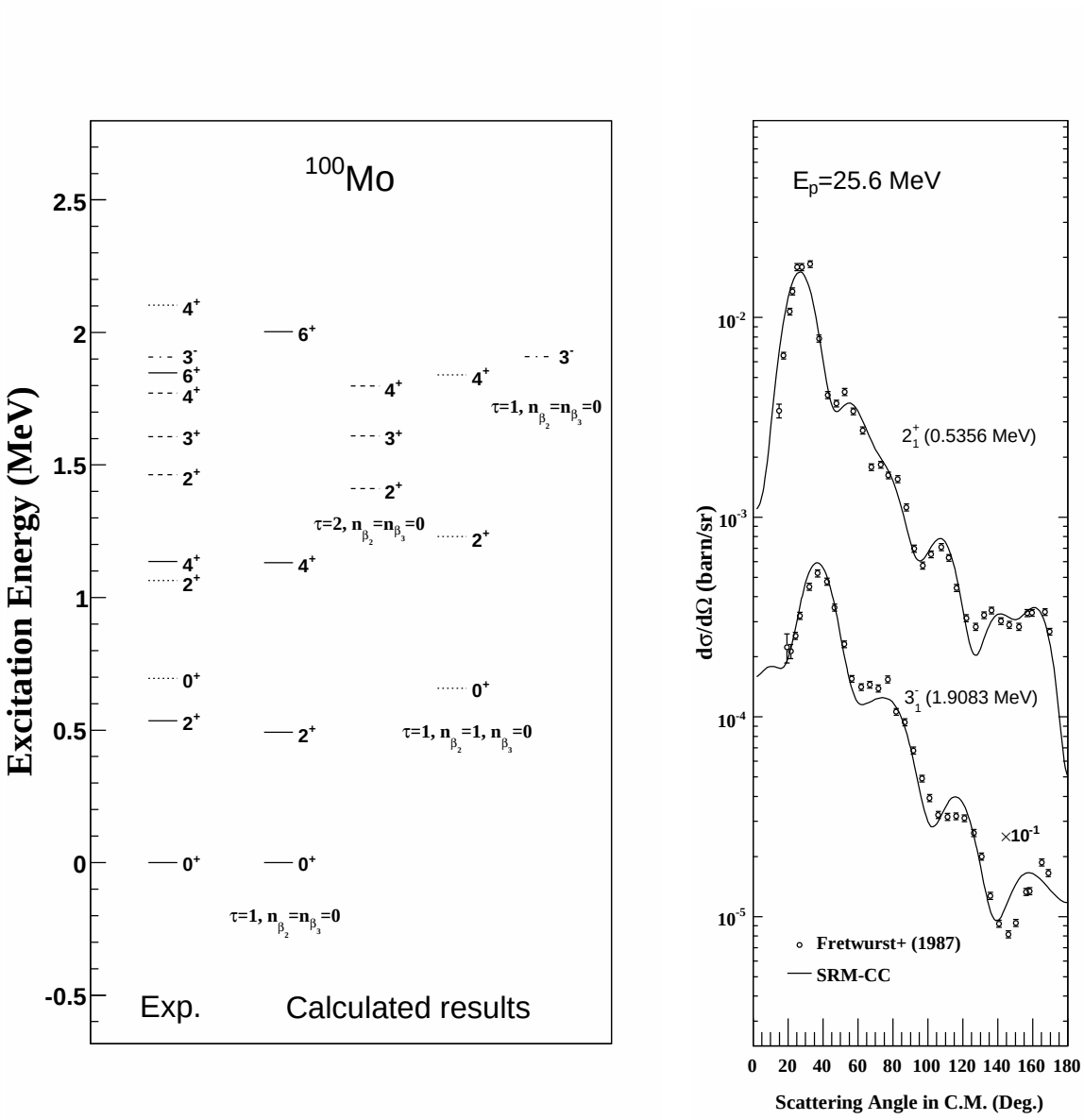

Fig. 4: The SRM(-CC) calculations obtained with the present Hamiltonian parameters which are compared to the experimental data for ^{100}Mo: The SRM low-lying level structure together with the experimental one (left) and the SRM-CC differential cross sections of inelastically-scattered protons at 25.6 MeV together with measured ones[31] (right)

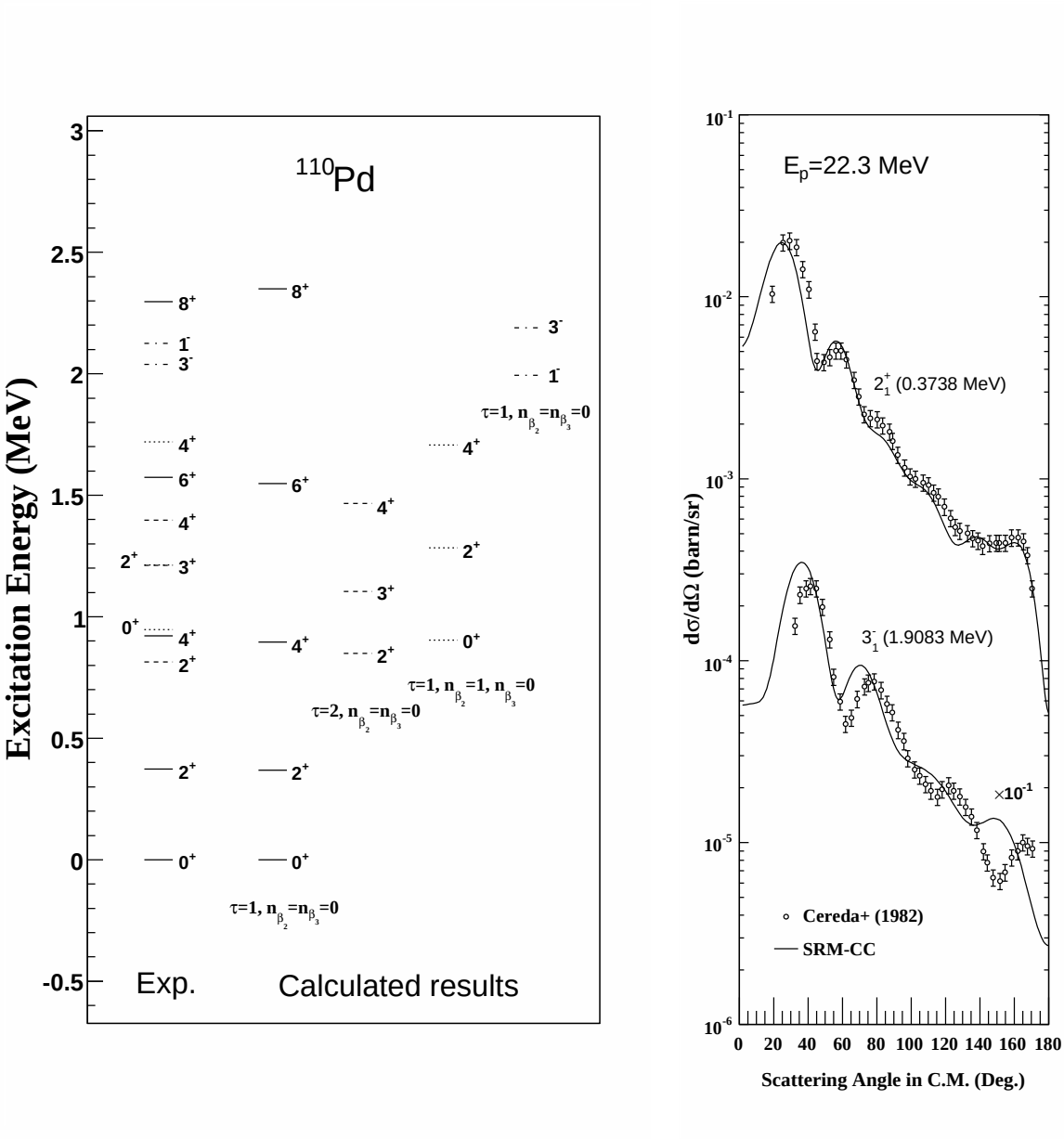

Fig. 5: The SRM(-CC) calculations obtained with the present Hamiltonian parameters which are compared to the experimental data for ^{110}Pd: The SRM low-lying level structure together with the experimental one (left) and the SRM-CC differential cross sections of inelastically-scattered protons at 22.3 MeV together with measured ones[32] (right)

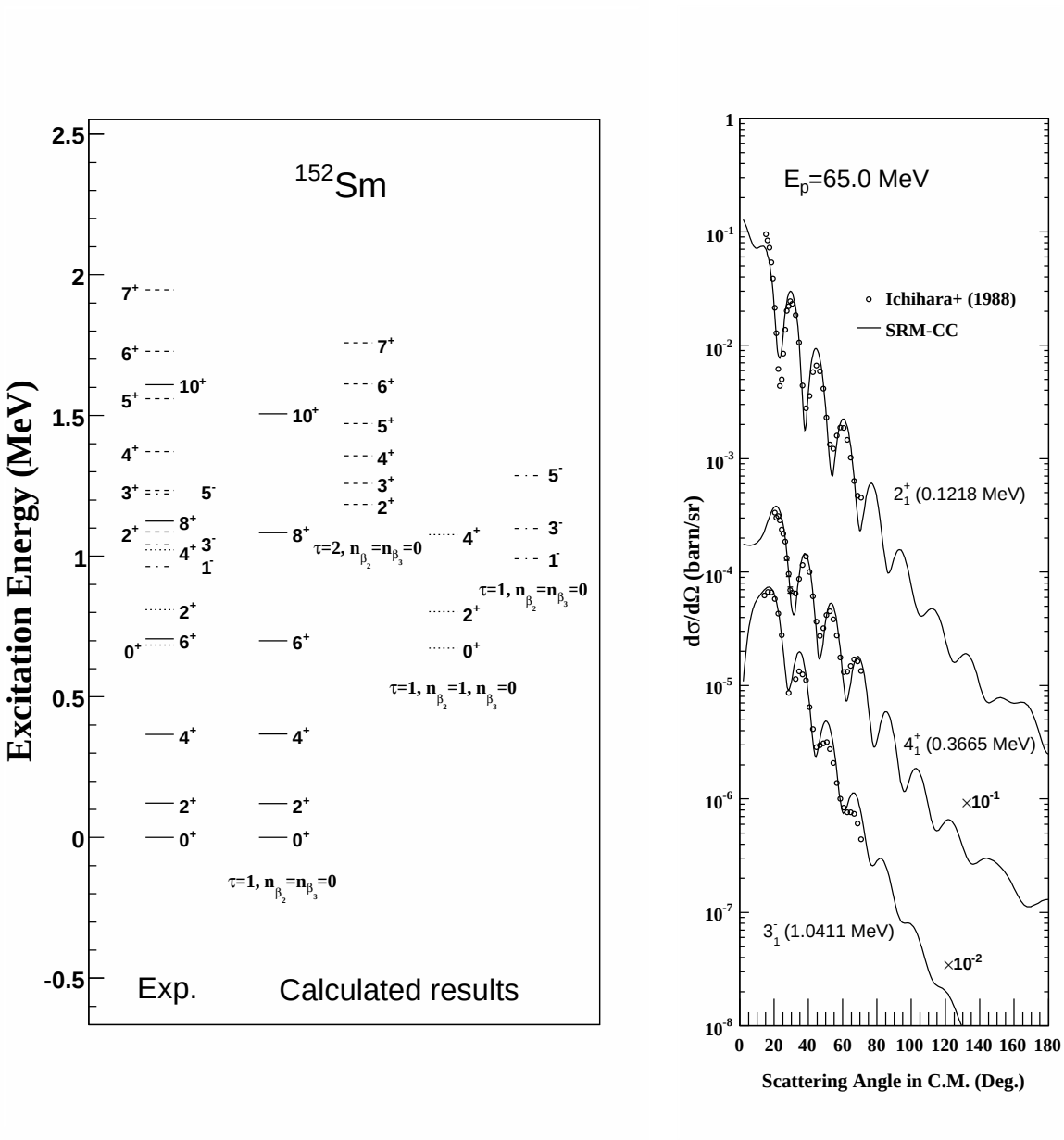

Fig. 6: The SRM(-CC) calculations obtained with the present Hamiltonian parameters which are compared to the experimental data for ^{152}Sm: The SRM low-lying level structure together with the experimental one (left) and the SRM-CC differential cross sections of inelastically-scattered protons at 65.0 MeV together with measured ones[42] (right)

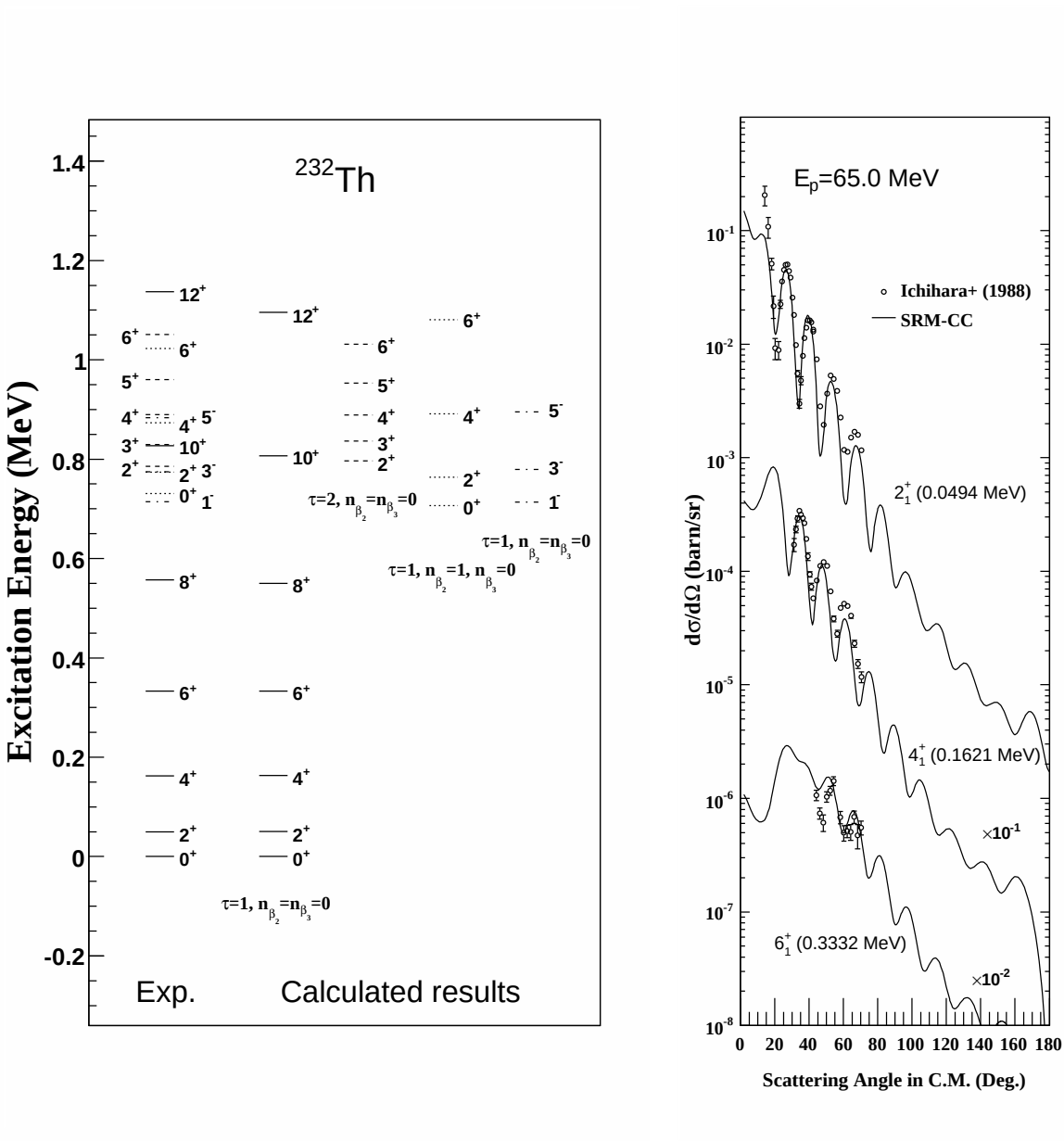

Fig. 7: The SRM(-CC) calculations obtained with the present Hamiltonian parameters which are compared to the experimental data for ^{232}Th: The SRM low-lying level structure together with the experimental one (left) and the SRM-CC differential cross sections of inelastically-scattered protons at 65.0 MeV together with measured ones[52] (right)

4 Deduced Hamiltonian Parameters

4.1 Isotopic Differences and Notable Phenomena

The obtained SRM Hamiltonian parameters are completely listed in **Table 3** for each isotope. We also illustrate the isotopic variances of the principal parameters which determine majority of the collective nature, i.e., the quadrupole and the octupole softness parameters $\mu_{\beta_{20}}$ and μ_ϵ in **Fig. 8**, the equilibrium deformation parameters β_{20} and β_{30} in **Fig. 9** and the quadrupole non-axial equilibrium deformation parameter γ_0 in **Fig. 10**. One can see varieties of parameter values as functions of neutron or proton numbers. Notable phenomena are reported and briefly discussed in the following subsections.

4.1.1 Lighter nuclei : ^{56}Fe - ^{86}Sr

This region is characterized by strong fluctuations of parameter values among the isotopes. For example, it is evident the value of β_{20} varies with large magnitudes of fluctuation between 0.05 and 0.25. Similarly, some anomalous behaviors are also seen for the value of $\mu_{\beta_{20}}$. They are supposed to be related with various configurations of neutrons and/or protons. One of the apparent irregular phenomena is seen between ^{56,58}Fe and ^{60,62,64}Ni where the value of $\mu_{\beta_{20}}$ increases and those for β_{20} suddenly decreases by an additional proton pair. There is no doubt that it is ascribed to the proton magic number $Z = 28$. It should be noted that the value of $\mu_{\beta_{20}}$ enlarges more at ^{68,70}Zn, ^{70,72}Ge and ^{74}Se. They are also characterized by very small equilibrium deformation parameters ~ 0.05, namely almost spherical shapes. These phenomena are consistent with a well known fact that a soft sub-shell closure exists at $N = 40$. It is amazing that the value of β_{20} drastically increases from 0.05 to 0.25 between ^{72}Ge and ^{74}Ge, and the value of $\mu_{\beta_{20}}$ comes down in contrast. The occupation of a strongly deformed $\nu g_{9/2}$ orbit is expected to produce such a drastic phenomenon. The neutron closed shell core $N = 50$ surely degrades the β_{20} value as we can see around ^{82}Se and ^{86}Sr.

The octupole softness constant parameter μ_ϵ seems to be not influenced by the closed shells so much, unlike the behavior of $\mu_{\beta_{20}}$. In contrast to this, the values of β_{30} are very similar to those for β_{20} both in magnitude and isotopic trend in many cases, namely, they reflect the closed shell effects. However, unusual phenomena are clearly found in typical quadrupole deformed nuclei ($\beta_{20} \gtrsim 0.2$), e.g., ^{74,76}Ge where the β_{30} values are not enhanced. This kind of tendency is also visible in ^{56,58}Fe and ^{76,78,80}Se. These facts may imply that equilibrium octupole deformation is related to the closed shells as the quadrupole one, but is not so involved with the largely deformed orbits.

The obtained γ_0 values vary from 15° to 35° in this mass region. They seems to be not strongly changed by the closed shells, instead, the values are almost constant or vary little by little with neutron and proton numbers though exceptional behaviors are visible at ^{62}Ni. It is interesting that many of these nuclei exhibit $\gamma_0 \sim 30°$, i.e., very middle shape between the typical prolate and the oblate deformations. As for Ge isotopes, present results are almost consistent with the measured date by Toh *et al.*[54]

and Sugawara *et al.*[55] Furthermore, recent Hartree-Fock-Bogoliubov and some Hartree-Fock plus BCS calculations[56] support our results for those isotopes.

4.1.2 Medium nuclei : ^{96}Mo - ^{130}Te

Anomalous behaviors of parameter values can be seen at ^{96,98,100}Mo and ^{116,118}Sn where the values of $\mu_{\beta_{20}}$ are enlarged, and those for β_{20} become exceedingly small. As for ^{116}Sn, the $\mu_{\beta_{20}}$ value reaches up to ~ 8.0, and the β_{20} value results in almost zero. The proton closed shell $Z = 50$ surely gives the nucleus a spherical shape and a strong vibrational character. It is interesting that additional neutron pairs gradually decrease the value of $\mu_{\beta_{20}}$ and increase the value of β_{20} in $^{116-124}$Sn. It seems that the rotational-vibrational characters are given for $^{120-124}$Sn just like adjacent nuclei such as $^{104-110}$Pd, $^{106-116}$Cd and $^{122-130}$Te due to probable occupations of rather deformed neutron orbits. For ^{96,98,100}Mo, the situations are not necessarily the same as the cases for ^{116,118}Sn. It should be noted that the parameter values of ^{100}Mo are very different from those for ^{102}Ru, while the values are similar among the Mo isotopes. In spite of an only difference of a proton pair, it seems to bring a large influence to the collective nature. Contrary to this, pairs of neutrons seem not to affect the variance of the collective nature so much around those isotopes. Therefore, extremely small values of β_{20} (large values of $\mu_{\beta_{20}}$) are attributable to a spherical shell of protons rather than that of neutrons. Probably, splitting and lowering of the $\pi g_{9/2}$ orbit from $Z = 42$ to 44 would give rise to such a big change in the collectivity. The relatively rapid decrease of β_{20} in ^{126,128,130}Te may be ascribed to the neutron closed shell core $N = 82$.

As well as the cases for lighter nuclei, the μ_ϵ parameter seems to be not influenced by the closed shells so much. It is interesting that the values are almost equal to those for $\mu_{\beta_{20}}$ in ^{102}Ru, $^{104-110}$Pd, $^{106-116}$Cd and ^{120,122,124}Sn. Also, the parameter β_{30} are very similar to those for β_{20} both in magnitude and isotopic trend.

It is obvious that the values of γ_0 are classified into two groups. The values almost equal to 35° for ^{96,98,100}Mo and $^{116-124}$Sn while ^{102}Ru, $^{104-110}$Pd, $^{106-116}$Cd and $^{122-130}$Te exhibit $\gamma_0 \sim 20°$. The former nuclei have spherical shells, and the later ones can be considered to possess rather deformed shells. Therefore, one can expect that the γ_0 value is related to those shell properties of neutrons and/or protons for medium nuclei.

4.1.3 Heavier nuclei : ^{144}Nd - ^{194}Pt together with ^{232}Th and ^{238}U

The most of these nuclei are characterized by very small $\mu_{\beta_{20}}$ ($0.2 \lesssim \mu_{\beta_{20}} \lesssim 0.3$) and very large β_{20} values ($0.20 \lesssim \beta_{20} \lesssim 0.28$). Thus they are typical rotational (deformed) nuclei (at least in the low-lying states) unlike the lighter ones. A steep difference of the β_{20} value can be seen between ^{150}Sm and ^{152}Sm. It is consistent with a well known shape transition corresponding to a U(5) to SU(3) transition in IBM. Since the all parameter values of ^{152}Sm are quite similar to those for ^{150}Nd, it makes sense that the

equilibrium (and collective) properties depend strongly on the neutron number rather than the proton one around these nuclei attributable to filling of $\nu f_{7/2}$ orbit. The value of β_{20} is relatively small (~ 0.1) at ^{144}Nd and ^{148,150}Sm due to the neutron shell shell of $N = 82$. Similarly, rather small (~ 0.15) β_{20} values for ^{192}Os and ^{194}Pt are ascribed to the closed shell cores of protons $Z = 82$ and/or neutrons $N = 126$.

There can not be seen any special trends which are involved with the closed shell cores for the μ_ϵ values, and they are similar in values and trends to the $\mu_{\beta_{20}}$ values even in the shape transitional region. One should bear in mind that this tendency is also observed in the lighter and the medium nuclei. In ^{144,148}Nd and $^{148-154}$Sm, the value of β_{30} gradually decreases with neutron numbers, and then it becomes ~ 0.05 almost constantly. Also, we can see very big gaps between the values of β_{20} and β_{30} for many nuclei of this mass region. Though the deformed neutron shells should cause the large value of β_{20}, those deformed orbits are hardly involved in the equilibrium octupole deformation. A similar phenomena is also seen typically in ^{74,76}Ge as mentioned in (1).

The effects of the spherical shell cores are obvious on the γ_0 values in this heavier region. Actually, near spherical nuclei such as ^{144}Nd, ^{148}Sm, ^{192}Os and ^{194}Pt exhibit relatively large values ($20^\circ \lesssim \gamma_0 \lesssim 30^\circ$) while the values are constantly small ($\sim 10^\circ$) for deformed nuclei. It is presumable that an apparent isotopic variance is seen in a typical shape transitional region, i.e., $^{148-154}$Sm. So we can expect that the γ_0 parameter is related to magnitude of β_{20}, namely the shell structures of neutrons and protons as well as for the medium nuclei.

4.1.4 Overall remarks

The anomalous behaviors of the quadrupole softness parameter $\mu_{\beta_{20}}$ and the equilibrium deformation parameter β_{20} can be explained by the varieties of the shell structure. In general, the values of β_{20} decrease if those for $\mu_{\beta_{20}}$ increase, and vice versa. The closed shells give very large $\mu_{\beta_{20}}$ and exceedingly small β_{20} values. In contrast, the deformed valence shells produce rather small $\mu_{\beta_{20}}$ and enlarge β_{20} values. The octupole softness parameter μ_ϵ is not so enhanced by the spherical shells unlike the case for the quadrupole parameter $\mu_{\beta_{20}}$. However, except for the spherical nuclei, the values show behaviors analogous to those for $\mu_{\beta_{20}}$. The equilibrium octupole deformation parameter β_{30} behaves like β_{20} for near spherical nuclei, but it dose not tend to be enlarged exceedingly by typically deformed shells. As for the non-axial quadrupole deformation parameter γ_0, it seems to correlate very closely with the β_{20} parameter especially for medium and heavier nuclei. It is noticeable that the parameter always results in the values between 10° and around 30°. In Sec. 4.3, we would like to show overall systematic trends among those parameter values.

Table 3: The nuclear Hamiltonian parameters obtained in the present SRM and SRM-CC analyses for various even-even nuclei

Nuc. (ϵ_{42})	$\hbar\omega_0$	$\mu_{\beta_{20}}$	γ_0	μ_ϵ	η	a_{32}	δ_n	γ_4	δ_4	a_{42}	β_{20}	β_{30}	β_{40}
^{56}Fe (2.46)	2.5564	0.5544	0.2979 (17.07°)	0.7012	0.7140	0.13806	6.3620				0.240	0.169	
^{58}Fe (2.56)	1.6960	0.7429	0.3937 (22.56°)	0.6135	1.1925	0.15993	6.4579				0.210	0.174	
^{60}Ni (1.88)	1.4280	1.3027	0.5205 (29.82°)	0.3899	0.4363	0.01760	5.8233				0.115	0.098	
^{62}Ni (1.99)	1.2314	1.8919	0.3201 (18.34°)	0.4127	0.6716	0.01019	5.7744				0.110	0.092	
^{64}Ni (1.94)	2.2007	0.7105	0.5439 (31.16°)	0.2983	0.7639	0.01734	3.1423				0.165	0.146	
^{64}Zn (2.33)	1.2250	1.2400	0.4776 (27.36°)	0.9910	0.5325	0.26783	4.3257				0.130	0.112	
^{66}Zn (2.36)	1.6495	0.9169	0.5177 (29.66°)	1.1867	0.6564	0.20158	2.8623				0.145	0.146	
^{68}Zn (2.24)	0.8424	2.5286	0.6078 (34.82°)	1.3433	0.6389	0.06293	4.1421				0.059	0.055	
^{70}Zn (2.02)	0.5857	3.5888	0.6195 (35.49°)	1.1047	0.4216	0.04692	9.3621				0.048	0.056	
^{70}Ge (2.07)	0.6685	2.6466	0.4783 (27.40°)	0.8663	1.1904	0.07437	6.2696				0.062	0.084	
^{72}Ge (2.07)	0.3846	3.9290	0.4576 (26.22°)	1.2470	0.8157	0.12363	17.6756				0.044	0.069	
^{74}Ge (2.46)	1.1985	0.6835	0.4529 (25.95°)	0.5097	0.0676	0.04585	6.6602				0.245	0.114	
^{76}Ge (2.50)	1.7521	0.4719	0.4854 (27.81°)	0.4974	0.0950	0.03355	6.2196				0.265	0.115	
^{74}Se (2.15)	0.5266	2.2833	0.4077 (23.36°)	1.0263	0.5935	0.06692	11.0532				0.090	0.105	
^{76}Se (2.38)	0.7632	1.0983	0.3903 (22.36°)	0.4139	1.0436	0.08881	7.6818				0.180	0.127	

table continued on next page

continued from previous page

Nuc. (ϵ_{42})	$\hbar\omega_0$	$\mu_{\beta_{20}}$	γ_0	μ_ϵ	η	a_{32}	δ_n	γ_4	δ_4	a_{42}	β_{20}	β_{30}	β_{40}
^{78}Se (2.45)	1.0296	0.8849	0.3778 (21.65°)	0.8244	1.0372	0.12338	6.0380				0.195	0.121	
^{80}Se (2.55)	1.0274	0.9858	0.3949 (22.63°)	0.6246	0.8826	0.13103	6.7206				0.165	0.114	
^{82}Se (2.65)	0.8854	1.2653	0.3496 (20.03°)	0.8403	0.6970	0.22146	6.8115				0.100	0.070	
^{86}Sr (2.07)	1.4859	0.9005	0.5707 (32.70°)	1.2221	0.2840	0.01348	2.2641				0.095	0.100	
^{96}Mo (2.09)	0.6468	2.4153	0.6159 (35.29°)	1.0647	0.4021	0.03705	6.1239				0.060	0.066	
^{98}Mo (1.92)	0.3953	5.1423	0.6226 (35.67°)	1.3970	0.4021	0.05047	9.5101				0.027	0.042	
^{100}Mo (2.12)	0.3519	4.2366	0.6500 (37.24°)	1.0113	0.4083	0.03997	13.0171				0.042	0.048	
^{102}Ru (2.33)	0.6299	1.1548	0.3812 (21.84°)	0.9013	0.7368	0.09404	9.1559				0.155	0.118	
^{104}Pd (2.38)	0.8924	0.9411	0.3763 (21.56°)	0.7411	0.5364	0.17696	6.4268				0.155	0.099	
^{106}Pd (2.40)	0.7402	1.0128	0.3950 (22.63°)	0.6757	0.6439	0.15712	7.2041				0.155	0.108	
^{108}Pd (2.42)	0.7244	0.8690	0.3831 (21.95°)	0.8248	1.0267	0.11399	8.2185				0.170	0.128	
^{110}Pd (2.46)	0.6571	0.8416	0.3631 (20.80°)	0.8773	0.9972	0.12687	12.3301				0.185	0.134	
^{106}Cd (2.36)	1.4477	0.6157	0.3485 (19.97°)	0.5530	0.5295	0.04251	4.5498				0.165	0.166	
^{108}Cd (2.38)	1.3671	0.6789	0.3658 (20.96°)	0.5873	0.5688	0.08995	3.7086				0.130	0.128	
^{110}Cd (2.34)	1.0616	0.8783	0.3805 (21.80°)	0.8641	0.6860	0.09002	3.8407				0.130	0.108	

table continued on next page

continued from previous page

Nuc. (ϵ_{42})	$\hbar\omega_0$	$\mu_{\beta_{20}}$	γ_0	μ_ϵ	η	a_{32}	δ_n	γ_4	δ_4	a_{42}	β_{20}	β_{30}	β_{40}
^{112}Cd (2.29)	0.8068	1.1510	0.3860 (22.12°)	0.9886	0.6525	0.06652	4.9524				0.110	0.079	
^{114}Cd (2.30)	0.7709	1.0353	0.3812 (21.84°)	0.8527	0.7864	0.06276	5.6407				0.125	0.117	
^{116}Cd (2.37)	0.9448	0.8128	0.3332 (19.09°)	1.0917	0.9885	0.10249	5.0521				0.140	0.109	
^{116}Sn (1.85)	0.9522	7.7847	0.5975 (34.23°)	1.6149	1.1751	0.00500	1.1078				0.013	0.016	
^{118}Sn (1.85)	0.9522	5.4448	0.5946 (34.07°)	1.6147	1.1542	0.00500	1.7171				0.018	0.022	
^{120}Sn (1.87)	1.0986	2.0927	0.6034 (34.57°)	1.6680	0.0000	0.00500	1.9822				0.045	0.055	
^{122}Sn (1.88)	1.2852	1.3106	0.6248 (35.80°)	1.5587	0.0000	0.00500	2.1083				0.062	0.067	
^{124}Sn (1.86)	1.3629	1.1203	0.6246 (35.79°)	1.4857	0.0000	0.00500	2.3750				0.065	0.076	
^{122}Te (2.09)	1.0709	0.6961	0.3650 (20.91°)	0.3852	0.8420	0.04552	5.5635				0.160	0.117	
^{124}Te (2.07)	1.4155	0.5583	0.3967 (22.73°)	0.4213	0.7850	0.03536	5.0885				0.160	0.126	
^{126}Te (2.04)	1.6336	0.5484	0.3892 (22.30°)	0.2476	0.7859	0.04263	4.0000				0.145	0.112	
^{128}Te (2.01)	1.6783	0.5745	0.4095 (23.46°)	0.8554	0.7312	0.04023	3.9606				0.125	0.081	
^{130}Te (1.95)	1.5559	0.6614	0.4363 (25.00°)	0.8415	0.7097	0.04337	3.8110				0.085	0.056	
^{144}Nd (1.89)	1.8215	0.4850	0.3710 (21.26°)	0.5000	0.6982	0.00973	1.1872				0.110	0.121	
^{150}Nd (2.93)	0.6668	0.4240	0.2086 (11.95°)	0.3256	0.1044	0.04521	7.8322	0.0346	0.5536	0.0053	0.235	0.065	0.065
^{148}Sm (2.14)	0.9646	0.7405	0.3271 (18.74°)	0.4887	0.3350	0.01851	1.3638				0.115	0.104	

table continued on next page

continued from previous page

Nuc. (ϵ_{42})	$\hbar\omega_0$	$\mu_{\beta_{20}}$	γ_0	μ_ϵ	η	a_{32}	δ_n	γ_4	δ_4	a_{42}	β_{20}	β_{30}	β_{40}
^{150}Sm (2.32)	0.4592	1.1802	0.2518 (14.43°)	1.0045	0.1596	0.05293	5.3291				0.120	0.084	
^{152}Sm (3.01)	0.6464	0.4322	0.1841 (10.55°)	0.3182	0.0971	0.04812	10.0354	0.0000	0.3366	0.0191	0.235	0.067	0.065
^{154}Sm (3.25)	1.0675	0.2694	0.1510 (08.65°)	0.3161	0.0000	0.02430	11.7431	0.3134	0.2704	0.0017	0.240	0.053	0.080
^{160}Gd (3.30)	1.2937	0.2316	0.1642 (09.41°)	0.3107	0.8915	0.01561	17.1220	0.8872	2.7085	0.0004	0.280	0.083	-0.080
^{164}Dy (3.30)	1.5227	0.2116	0.2085 (11.95°)	0.2350	0.0000	0.01907	13.2444	1.7000	2.4254	0.0040	0.260	0.053	-0.045
^{166}Er (3.29)	1.4305	0.2230	0.2150 (12.32°)	0.2350	0.0000	0.00771	19.8983	1.7297	0.7291	0.0012	0.262	0.053	0.040
^{168}Er (3.31)	1.1832	0.2478	0.2090 (11.97°)	0.2067	0.0000	0.00785	18.7592	1.7440	0.7258	0.0013	0.260	0.061	-0.040
^{174}Yb (3.31)	1.4740	0.2461	0.1422 (08.15°)	0.2444	0.1470	0.02962	14.3824	0.5014	0.7551	0.0576	0.260	0.052	-0.045
^{176}Yb (3.31)	1.1233	0.2640	0.1530 (08.77°)	0.2092	0.1070	0.00632	14.1420	0.4590	0.2679	0.0093	0.245	0.059	-0.060
^{178}Hf (3.29)	1.1658	0.2845	0.1861 (10.66°)	0.2809	0.0000	0.05978	13.4030	0.1821	0.2954	0.0073	0.235	0.062	-0.050
^{180}Hf (3.31)	1.0908	0.3084	0.1660 (09.51°)	0.3273	0.0390	0.08138	12.6714	0.1751	0.3056	0.0249	0.235	0.086	-0.050
^{182}W (3.29)	1.1428	0.2984	0.1904 (10.91°)	0.2646	0.0000	0.05744	13.0550	0.2492	0.3546	0.0070	0.230	0.070	-0.060
^{184}W (3.27)	0.9917	0.3341	0.2413 (13.83°)	0.3739	0.0000	0.03322	11.1564	0.2522	0.5288	0.0199	0.220	0.077	-0.070

table continued on next page

continued from previous page

Nuc. (ϵ_{42})	$\hbar\omega_0$	$\mu_{\beta_{20}}$	γ_0	μ_ϵ	η	a_{32}	δ_n	γ_4	δ_4	a_{42}	β_{20}	β_{30}	β_{40}
^{192}Os (2.82)	0.8974	0.4754	0.4063 (23.28°)	0.3023	0.0000	0.07240	6.8535	0.6656	0.0000	0.0454	0.160	0.048	-0.065
^{194}Pt (2.47)	1.1579	0.4865	0.5200 (29.79°)	0.6058	0.0000	0.05071	5.0092	0.0319	0.0000	0.0096	0.150	0.039	-0.060
^{232}Th (3.28)	0.7063	0.2649	0.1734 (09.94°)	0.4203	0.0000	0.00409	14.7019	0.1323	0.7051	0.0311	0.240	0.066	0.080
^{238}U (3.31)	0.9881	0.2135	0.1437 (08.23°)	0.4567	0.0032	0.00200	14.8800	0.0746	0.7030	0.0259	0.250	0.039	0.070

- The symbol ϵ_{42} stands for the level energy ratio $E(4_1^+)/E(2_1^+)$.
- The value of $\hbar\omega_0$ and δ_n are described in MeV.

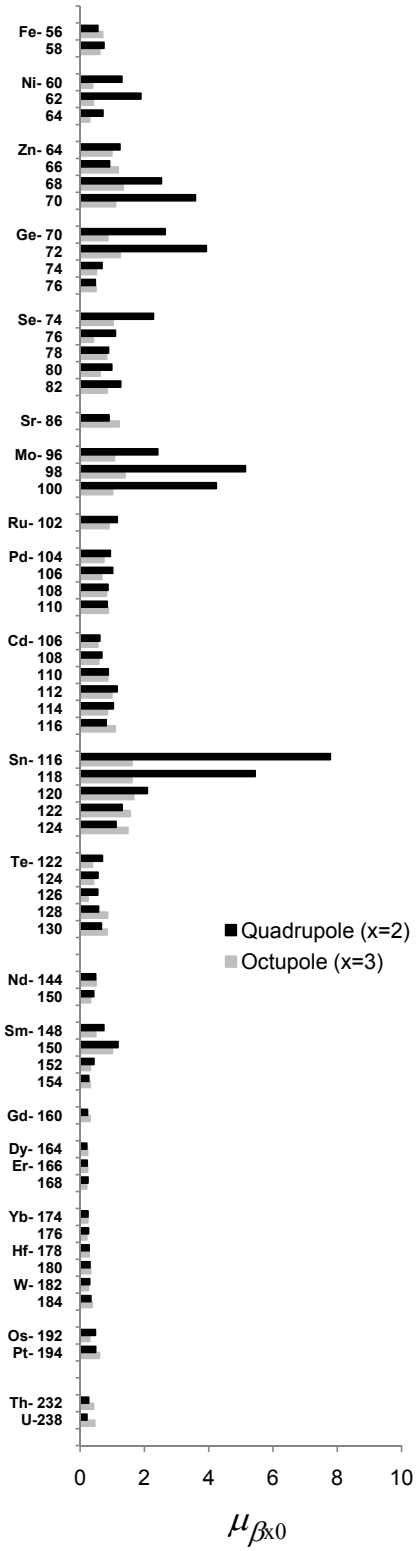

Fig. 8: Isotopic variance of the softness parameters $\mu_{\beta_{20}}$ and μ_ϵ

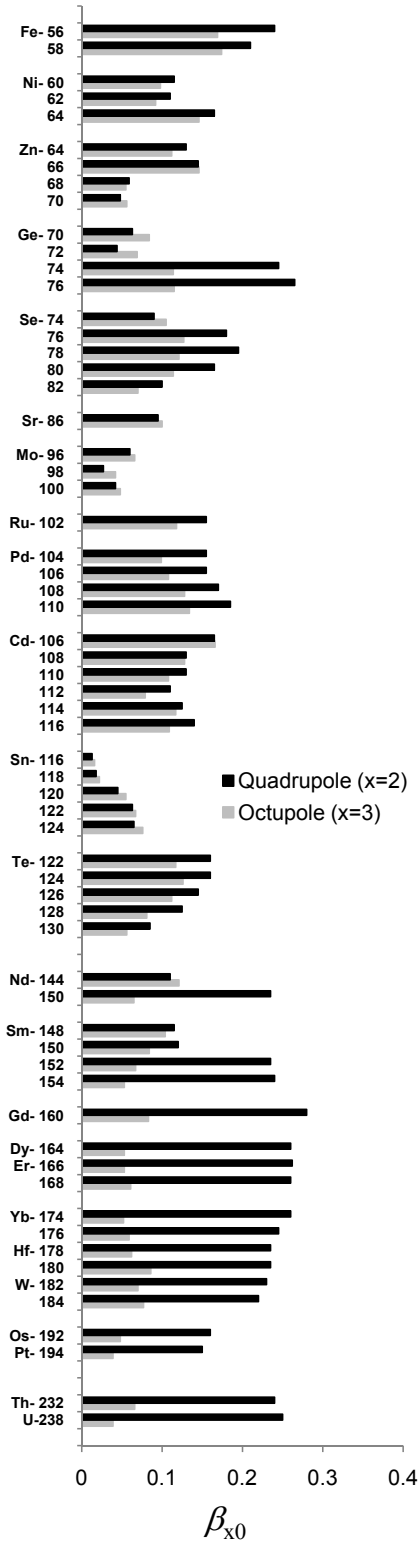

Fig. 9: Isotopic variance of the equilibrium deformation parameters β_{20} and β_{30}

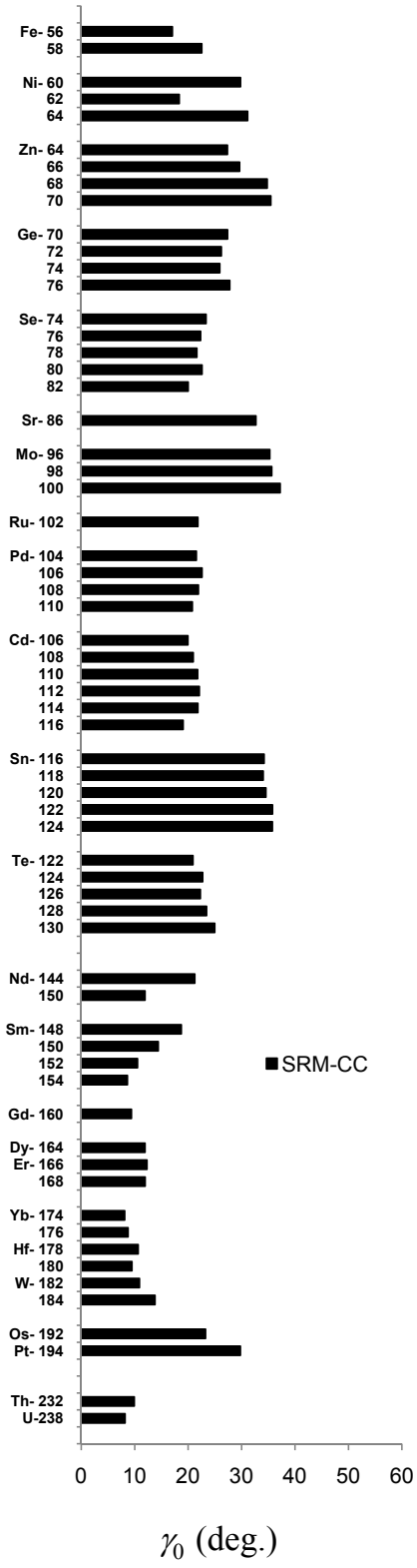

Fig. 10: Isotopic variance of the quadrupole non-axial equilibrium deformation parameter γ_0

4.2 Comparisons with the Experimental and the Mass-model Results

The quadrupole deformation parameters had been deduced by Raman *et al.*[57] from the measured electric-quadrupole transition probabilities $B(E2; 0_1^+ \rightarrow 2_1^+)$ for various even-even isotopes. Similarly, the octupole deformation had also been extracted by Kibedi and Spear[58] from the measured electric-octupole transition probabilities $B(E3; 0_1^+ \rightarrow 3_1^-)$. Also, some mass-models have predicted the static deformations systematically. Thus our results should be compared with those values in order to survey the validity of present analyses. Note that the experimental values correspond to the "effective" deformation which attributes to both the rotation and the vibration, while the mass-models predict equilibrium G.S. deformations. So we calculated the effective quadrupole deformation $\beta_2^{eff.} \equiv \langle 0_1^+|\beta_2|2_1^+\rangle$, and the effective octupole deformation $\beta_3^{eff.} \equiv \langle 0_1^+|\beta_3|3_1^-\rangle$ which described the strengths of exciting 2_1^+ and 3_1^-, respectively. The SRM-CC results are compared with those experimental and mass-model values in **Table 4** and in **Figs. 11-15**. We picked up the predicted values of the Finite Range Droplet Model (FRDM)[59], a Hartree-Fock-Bogolubov (HFB) method[60] and the Koura-Tachibana-Uno-Yamada (KTUY) model[61].

The obtained quadrupole and octupole effective-deformations reproduce the experimental data well aside from some exceptions. It is no wonder that the calculated effective deformations tend to be enormously larger than the equilibrium G.S. deformations for the typical vibrational nuclei, while those two values are almost equal for the typical rotational nuclei. The discrepancies can be seen for typically deformed heavy-nuclei such as ^{150}Nd, ^{152,154}Sm, ^{160}Gd, ^{164}Dy, ^{166,168}Er and ^{174,176}Yb, where the SRM-CC results underestimate measured values by $\sim 20\%$. However it should be noted that the deduced equilibrium G.S. deformation parameters (β_{20} and β_{40}) are almost consistent with the values obtained in the original CC analyses done by, e.g., Ichihara *et al.*[42] who employed simple but suitable models for such nuclei. The values of equilibrium G.S. quadrupole deformation β_{20} also describe gross tendency of the mass-models results, though there are some exceptional isotopes (or isotope regions). And one might see a fact that they become similar values in the deformed heavy region ($A \gtrsim 150$). Present results of β_{30} and β_{40} usually deviate from the mass-model results. We do not discuss them because it is difficult to determine these small values quantitatively by the mass-models in general.

Table 4: The equilibrium G.S. and the effective deformations derived from the SRM-CC analyses which are compared with the measured values (effective ones) and the mass-model predictions (equilibrium G.S. ones)

	Present SRM-CC Analyses						Measured Values		Mass-model Predictions								
							Raman[57]	Kibedi[58]	FRDM[59]				HFB[60]		KTUY05[61]		
	β_{20}	β_{30}	β_{40}	$\beta_2^{eff.}$	$\beta_3^{eff.}$	γ_0	$\beta_2^{eff.}$	$\beta_3^{eff.}$	β_2	β_3	β_4	β_6	β_2	β_4	β_2	β_4	β_6
^{56}Fe	0.240	0.169	0.000	0.263	0.181	17.07°	0.2392± 0.0049	0.196980	0.000	-0.028	0.000	0.000	0.160	-0.010	0.093	-0.001	-0.008
^{58}Fe	0.210	0.174	0.000	0.263	0.207	22.56°	0.2586± 0.0043	0.189507	0.199	0.000	-0.019	-0.001	0.130	-0.010	0.017	-0.001	-0.001
^{60}Ni	0.115	0.098	0.000	0.215	0.167	29.82°	0.2070± 0.0017	0.209084	0.027	0.000	0.000	0.000	-0.090	0.000	0.017	-0.001	-0.001
^{62}Ni	0.110	0.092	0.000	0.280	0.214	18.34°	0.1978± 0.0028	0.197463	-0.096	0.000	0.012	0.004	-0.200	-0.020	0.019	-0.001	0.000
^{64}Ni	0.165	0.146	0.000	0.203	0.178	31.16°	0.1790± 0.0090	0.200629	-0.087	0.000	-0.005	0.002	-0.170	-0.020	0.017	-0.001	-0.004
^{64}Zn	0.130	0.112	0.000	0.231	0.194	27.36°	0.2420± 0.0110	0.232787	0.219	0.000	-0.031	-0.008	-0.190	-0.020	0.103	0.027	-0.001
^{66}Zn	0.145	0.146	0.000	0.207	0.209	29.66°	0.2180± 0.0080	0.235481	-0.215	0.000	0.005	0.038	-0.200	-0.030	0.103	0.012	-0.006
^{68}Zn	0.059	0.055	0.000	0.195	0.172	34.82°	0.2050± 0.0120	0.231623	-0.156	0.000	-0.022	0.001	-0.180	-0.020	0.076	-0.005	-0.004
^{70}Zn	0.048	0.056	0.000	0.220	0.205	35.49°	0.2280± 0.0100	0.209680	0.045	0.000	0.001	0.001	0.000	0.000	0.013	0.000	0.000
^{70}Ge	0.063	0.084	0.000	0.215	0.259	27.40°	0.2245± 0.0026	0.273755	-0.241	0.000	-0.014	0.027	-0.240	-0.040	0.193	0.045	-0.003
^{72}Ge	0.044	0.069	0.000	0.219	0.217	26.22°	0.2424± 0.0034	0.264063	-0.224	0.000	-0.034	0.005	-0.210	-0.030	0.198	0.044	-0.008
^{74}Ge	0.245	0.114	0.000	0.295	0.129	25.95°	0.2825± 0.0028	0.144762	-0.224	0.000	-0.041	0.001	0.170	-0.010	0.182	0.022	-0.011
^{76}Ge	0.265	0.115	0.000	0.279	0.120	27.81°	0.2623± 0.0039	0.144433	0.143	0.000	0.008	-0.004	0.170	0.000	0.165	0.007	-0.019
^{74}Se	0.090	0.105	0.000	0.271	0.246	23.36°	0.3019± 0.0031	0.139611	-0.250	0.000	-0.029	0.017	-0.250	-0.050	0.245	0.028	-0.015
^{76}Se	0.180	0.127	0.000	0.293	0.184	22.36°	0.3090± 0.0037	0.167804	-0.241	0.000	-0.038	0.008	0.240	-0.020	0.220	0.002	-0.016
^{78}Se	0.195	0.121	0.000	0.272	0.159	21.65°	0.2712± 0.0036	0.150186	0.143	0.000	-0.017	0.003	0.190	-0.010	0.187	-0.020	-0.014
^{80}Se	0.165	0.114	0.000	0.248	0.158	22.63°	0.2318± 0.0027	0.154352	0.153	0.000	-0.024	0.002	0.140	-0.010	0.149	-0.039	-0.003
^{82}Se	0.100	0.070	0.000	0.180	0.117	20.03°	0.1934± 0.0027	0.145481	0.154	0.000	-0.049	0.013	0.000	0.000	0.082	-0.032	0.005
^{86}Sr	0.095	0.100	0.000	0.135	0.141	32.70°	0.1400± 0.0080	0.165355	0.053	0.000	-0.007	0.001	0.000	0.000	0.063	-0.020	0.000
^{96}Mo	0.060	0.066	0.000	0.191	0.186	35.29°	0.1720± 0.0016	0.182345	0.080	0.000	0.018	0.000	0.000	0.000	0.116	0.035	-0.002
^{98}Mo	0.027	0.042	0.000	0.174	0.215	35.67°	0.1683± 0.0028	0.214769	0.180	0.000	0.022	-0.020	0.000	0.000	0.152	0.034	-0.003
^{100}Mo	0.042	0.048	0.000	0.225	0.186	37.24°	0.2309± 0.0022	0.218242	0.244	0.000	0.023	-0.015	-0.200	-0.020	0.190	0.027	-0.008
^{102}Ru	0.155	0.118	0.000	0.262	0.170	21.84°	0.2404± 0.0019	0.137697	0.189	0.000	0.015	-0.020	0.210	-0.010	0.174	0.000	-0.019

table continued on next page

continued from previous page

	Present SRM-CC Analyses						Measured Values		Mass-model Predictions								
							Raman[57]	Kibedi[58]	FRDM[59]				HFB[60]		KTUY05[61]		
	β_{20}	β_{30}	β_{40}	$\beta_2^{eff.}$	$\beta_3^{eff.}$	γ_0	$\beta_2^{eff.}$	$\beta_3^{eff.}$	β_2	β_3	β_4	β_6	β_2	β_4	β_2	β_4	β_6
^{104}Pd	0.155	0.099	0.000	0.225	0.134	21.56°	0.2090± 0.0070	0.135955	0.162	0.000	0.002	-0.017	0.160	-0.010	0.139	-0.026	-0.008
^{106}Pd	0.155	0.108	0.000	0.237	0.151	22.63°	0.2290± 0.0060	0.177853	0.171	0.000	-0.013	-0.006	0.180	-0.010	0.146	-0.037	-0.003
^{108}Pd	0.170	0.128	0.000	0.235	0.159	21.95°	0.2430± 0.0060	0.161084	0.190	0.000	-0.011	0.000	0.200	-0.010	0.152	-0.041	-0.003
^{110}Pd	0.185	0.134	0.000	0.250	0.149	20.80°	0.2570± 0.0060	0.149963	0.218	0.000	-0.017	0.008	0.200	-0.010	0.149	-0.039	-0.005
^{106}Cd	0.165	0.166	0.000	0.189	0.187	19.97°	0.1732± 0.0042	0.190561	0.126	0.000	-0.002	-0.007	0.120	0.000	0.067	-0.014	-0.003
^{108}Cd	0.130	0.128	0.000	0.155	0.153	20.96°	0.1752± 0.0041	0.181093	0.135	0.000	-0.018	-0.003	0.150	-0.010	0.074	-0.025	0.000
^{110}Cd	0.130	0.108	0.000	0.181	0.147	21.80°	0.1770± 0.0039	0.155681	0.144	0.000	-0.033	0.005	0.150	-0.010	0.079	-0.035	0.007
^{112}Cd	0.110	0.079	0.000	0.186	0.126	22.12°	0.1862± 0.0037	0.152235	0.144	0.000	-0.033	0.009	0.150	-0.010	0.076	-0.033	0.007
^{114}Cd	0.125	0.117	0.000	0.195	0.170	21.84°	0.1903± 0.0035	0.160328	0.163	0.000	-0.040	0.012	0.150	-0.010	0.073	-0.025	0.001
^{116}Cd	0.140	0.109	0.000	0.185	0.138	19.09°	0.1906± 0.0034	0.137664	-0.241	0.000	-0.038	0.014	0.000	0.000	0.073	-0.026	0.000
^{116}Sn	0.013	0.016	0.000	0.121	0.154	34.23°	0.1118± 0.0016	0.151838	0.000	0.000	-0.008	0.000	0.000	0.000	0.010	0.000	0.000
^{118}Sn	0.018	0.022	0.000	0.120	0.151	34.07°	0.1105± 0.0021	0.139321	0.000	0.000	0.000	0.000	0.000	0.000	0.010	0.000	-0.003
^{120}Sn	0.045	0.055	0.000	0.126	0.151	34.57°	0.1075± 0.0011	0.136999	0.000	0.000	0.000	0.000	0.000	0.000	0.010	0.000	-0.003
^{122}Sn	0.063	0.067	0.000	0.117	0.125	35.80°	0.1036± 0.0011	0.120527	0.000	0.000	0.000	0.000	0.000	0.000	0.010	0.000	-0.002
^{124}Sn	0.065	0.076	0.000	0.108	0.125	35.79°	0.0953± 0.0011	0.105631	0.000	0.000	0.000	0.000	0.000	0.000	0.010	0.000	-0.003
^{122}Te	0.160	0.117	0.000	0.194	0.137	20.91°	0.1847± 0.0008	0.132357	-0.139	0.000	-0.001	0.008	0.000	0.000	0.070	0.035	0.003
^{124}Te	0.160	0.126	0.000	0.177	0.136	22.73°	0.1695± 0.0009	0.130222	-0.113	0.000	-0.010	0.000	0.000	0.000	0.070	0.035	0.003
^{126}Te	0.145	0.112	0.000	0.159	0.123	22.30°	0.1534± 0.0016	0.122699	-0.105	0.000	-0.019	-0.003	0.000	0.000	0.067	0.032	0.000
^{128}Te	0.125	0.081	0.000	0.139	0.090	23.46°	0.1363± 0.0011	0.103003	0.000	0.000	0.000	0.000	0.000	0.000	0.067	0.020	-0.008
^{130}Te	0.085	0.056	0.000	0.101	0.066	25.00°	0.1184± 0.0014	0.087831	0.000	0.000	0.000	0.000	0.000	0.000	0.055	0.008	-0.007
^{144}Nd	0.110	0.121	0.000	0.117	0.130	21.26°	0.1237± 0.0006	0.143875	0.000	0.000	0.000	0.000	0.000	0.000	0.043	0.021	0.000
^{150}Nd	0.235	0.065	0.065	0.242	0.067	11.95°	0.2853± 0.0021	0.113309	0.243	0.000	0.107	-0.003	0.240	0.020	0.147	0.064	0.003
^{148}Sm	0.115	0.104	0.000	0.144	0.131	18.74°	0.1423± 0.0030	0.158496	0.161	0.000	0.059	0.006	0.150	0.010	0.063	0.000	-0.009
^{150}Sm	0.120	0.084	0.000	0.205	0.136	14.43°	0.1931± 0.0021	0.145117	0.206	0.000	0.067	-0.012	0.200	0.010	0.119	0.047	0.004
^{152}Sm	0.235	0.067	0.065	0.242	0.067	10.55°	0.3064± 0.0027	0.094854	0.243	0.000	0.090	-0.007	0.260	0.020	0.160	0.080	0.014
^{154}Sm	0.240	0.053	0.080	0.241	0.054	8.65°	0.3410± 0.0020	0.080280	0.270	0.000	0.113	-0.005	0.270	0.020	0.188	0.087	0.013

table continued on next page

continued from previous page

	Present SRM-CC Analyses						Measured Values		Mass-model Predictions								
							Raman[57]	Kibedi[58]	FRDM[59]				HFB[60]		KTUY05[61]		
	β_{20}	β_{30}	β_{40}	$\beta_2^{eff.}$	$\beta_3^{eff.}$	γ_0	$\beta_2^{eff.}$	$\beta_3^{eff.}$	β_2	β_3	β_4	β_6	β_2	β_4	β_2	β_4	β_6
^{160}Gd	0.280	0.083	-0.080	0.281	0.084	9.41°	0.3534± 0.0020	0.082340	0.280	0.000	0.065	-0.019	0.280	0.000	0.230	0.065	-0.016
^{164}Dy	0.260	0.053	-0.045	0.261	0.054	11.95°	0.3481± 0.0016	0.066431	0.292	0.000	0.025	-0.021	0.290	-0.010	0.238	0.053	-0.022
^{166}Er	0.262	0.053	0.040	0.263	0.054	12.32°	0.3420± 0.0015	0.053036	0.283	0.000	0.006	-0.019	0.320	-0.030	0.232	0.038	-0.029
^{168}Er	0.260	0.061	-0.040	0.261	0.062	11.97°	0.3381± 0.0029	0.043998	0.294	0.000	-0.007	-0.025	0.300	-0.020	0.251	0.032	-0.028
^{174}Yb	0.260	0.052	-0.045	0.261	0.053	8.15°	0.3249± 0.0016	0.059703	0.287	0.000	-0.059	-0.018	0.300	-0.040	0.257	-0.011	-0.025
^{176}Yb	0.245	0.059	-0.060	0.246	0.059	8.77°	0.3050± 0.0050	0.024097	0.278	0.000	-0.071	-0.009	0.290	-0.040	0.259	-0.028	-0.026
^{178}Hf	0.235	0.062	-0.050	0.236	0.062	10.66°	0.2803± 0.0017	0.043542	0.278	0.000	-0.080	-0.004	0.290	-0.050	0.252	-0.029	-0.021
^{180}Hf	0.235	0.086	-0.050	0.237	0.086	9.51°	0.2738± 0.0035	0.025781	0.279	0.000	-0.096	-0.002	0.210	-0.030	0.248	-0.047	-0.016
^{182}W	0.230	0.070	-0.060	0.232	0.070	10.91°	0.2508± 0.0024	0.049942	0.259	0.000	-0.084	0.001	0.230	-0.040	0.241	-0.041	-0.014
^{184}W	0.220	0.077	-0.070	0.222	0.078	13.83°	0.2362± 0.0041	0.050977	0.240	0.000	-0.095	0.010	0.240	-0.050	0.224	-0.062	0.000
^{192}Os	0.160	0.048	-0.065	0.168	0.050	23.28°	0.1667± 0.0012	0.060123	0.155	0.000	-0.081	0.020	-0.140	-0.030	-0.207	-0.007	0.021
^{194}Pt	0.150	0.039	-0.060	0.159	0.041	29.79°	0.1426± 0.0010	0.055721	-0.148	0.000	-0.029	0.007	0.000	0.000	-0.163	-0.028	0.014
^{232}Th	0.240	0.066	0.080	0.241	0.066	9.94°	0.2608± 0.0014	0.085307	0.207	0.000	0.108	0.003	0.210	0.030	0.182	0.072	0.001
^{238}U	0.250	0.039	0.070	0.250	0.040	8.23°	0.2863± 0.0024	0.084308	0.215	0.000	0.093	-0.015	0.240	0.020	0.204	0.054	-0.014

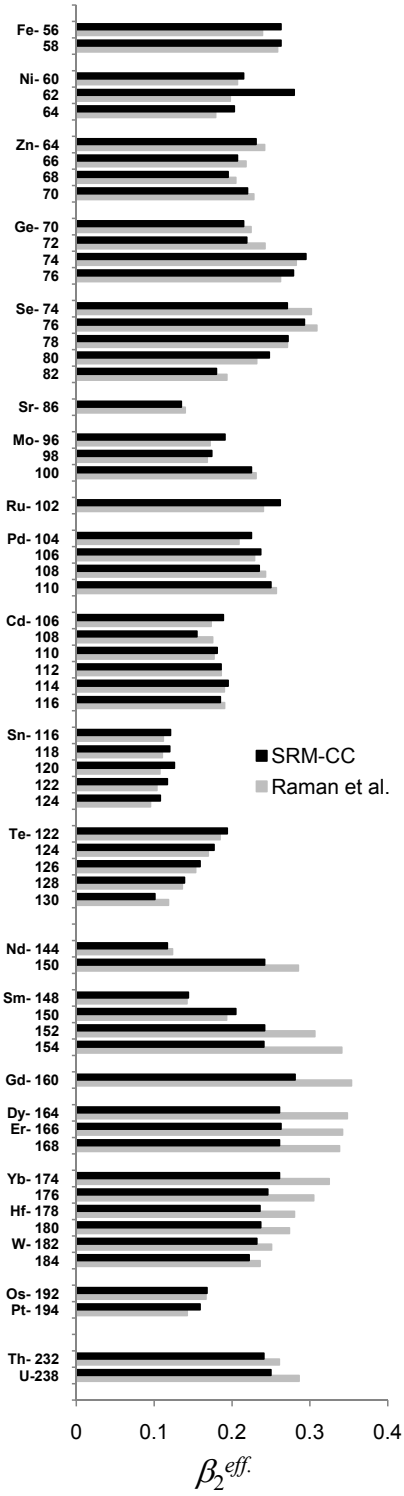

Fig. 11: Values of the effective quadrupole deformation parameter compared with experimental data compiled by Raman *et al.*[57].

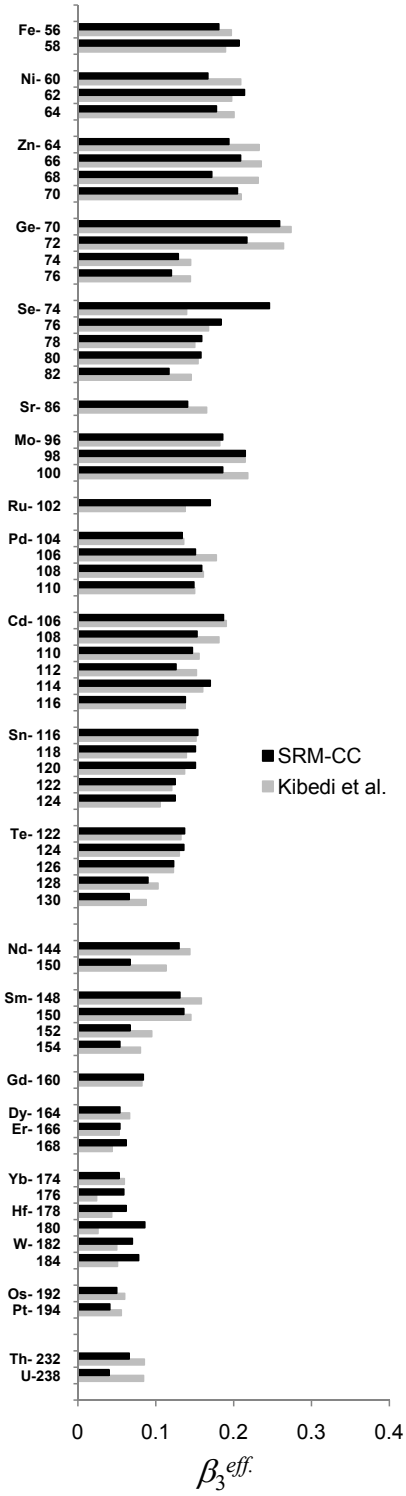

Fig. 12: Values of the effective octupole deformation parameter compared with experimental data compiled by Kibedi and Spear[58]

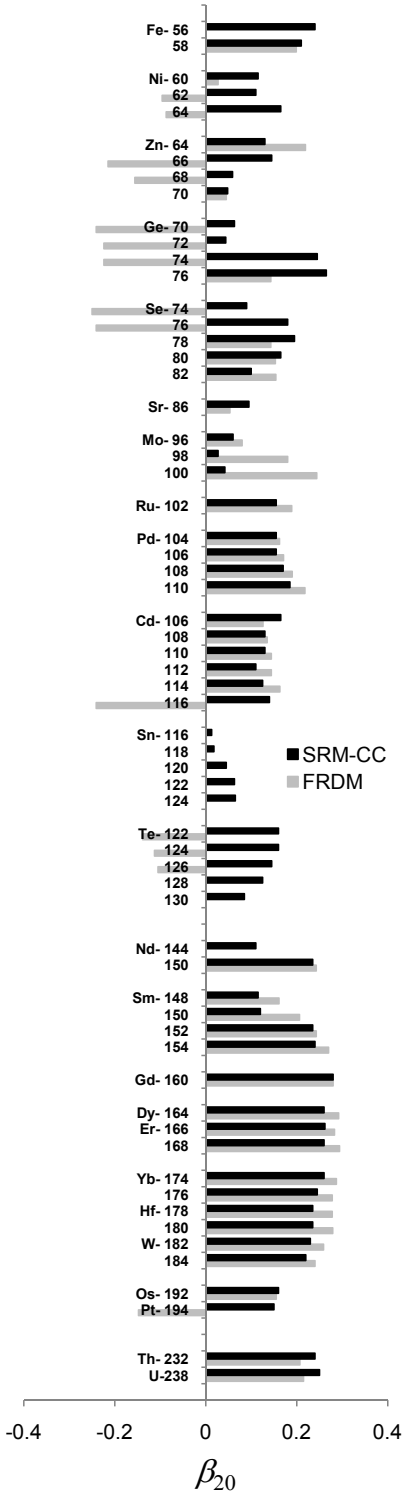

Fig. 13: Values of the equilibrium quadrupole deformation parameter compared with theoretical values calculated by FRDM[59]

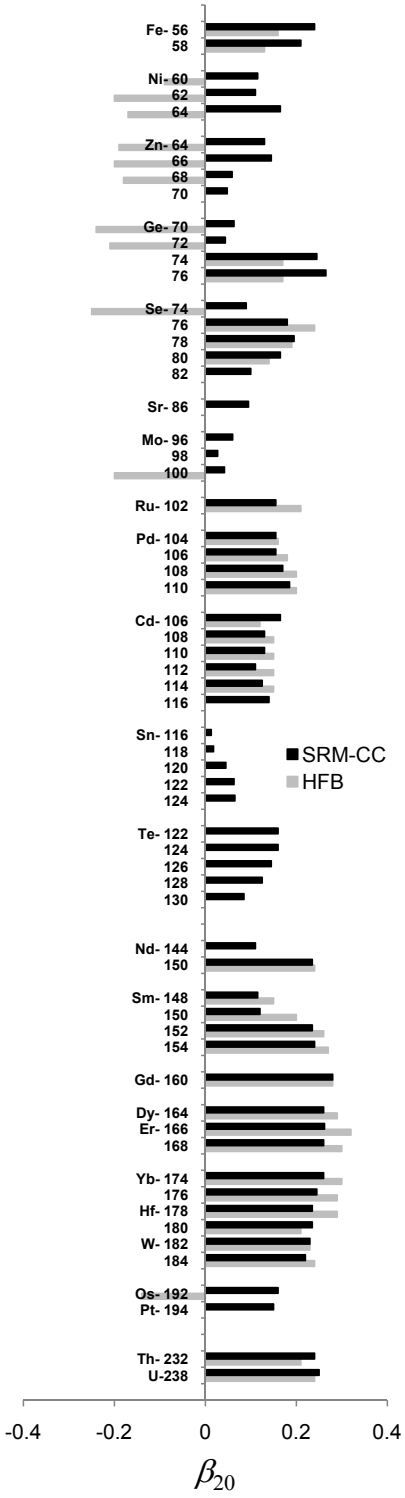

Fig. 14: Values of the equilibrium quadrupole deformation parameter compared with theoretical values calculated by the HFB method[60]

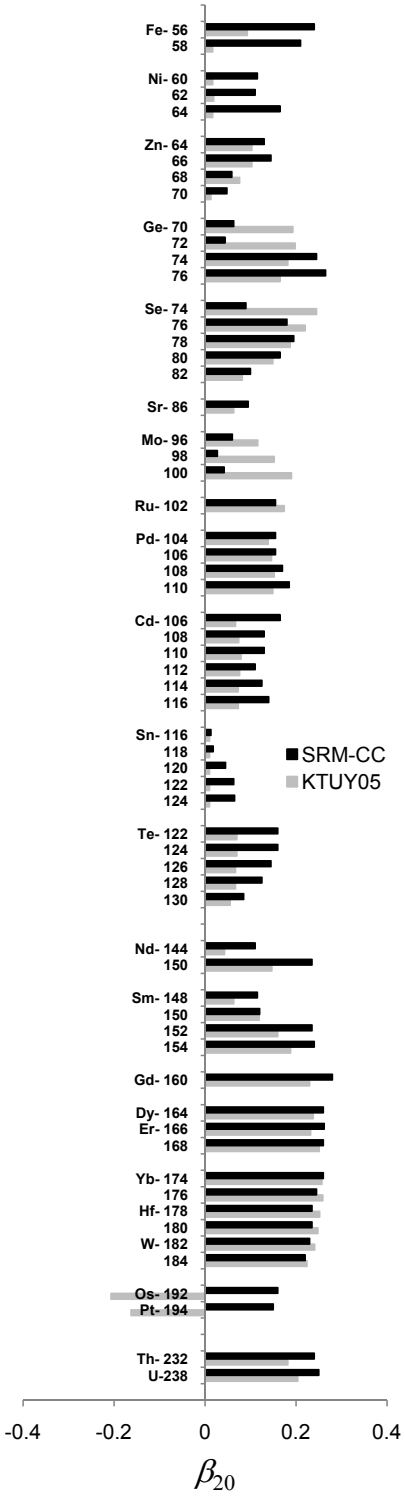

Fig. 15: Values of the equilibrium quadrupole deformation parameter compared with theoretical values calculated by the KTUY model[61]

4.3 Systematic Trends

According to our investigations, systematic trends can be seen among the major Hamiltonian parameters such as β_{20}, $\mu_{\beta_{20}}$, γ_0, β_{30} and μ_ϵ as shown in **Figs. 16**-(a), -(b), -(c) and -(d).

Here, the equilibrium G.S. deformation was represented as the deformation length $\delta_{l0} = 1.21A^{1/3}\beta_{l0}$ fm ($l = 2, 3$) in order to express it as its absolute value. Though the obtained results show some visible fluctuations, the existence of regular behaviors indicate the possibility that we can predict the collective natures and/or the low-lying level structures for many even-even nuclei by this kind of phenomenological model analysis. Following items are devoted to present features of each trend.

- Figure 16-(a) shows deduced values of $\mu_{\beta_{20}}$ as a function of the δ_{20} values for all nuclides investigated in this analysis. We can see an apparent systematic trend between the parameters where it is expected to present a transitional behavior of the rotational-vibrational motion. The parameter $\mu_{\beta_{20}}$ becomes very large at around $\delta_{20} \lesssim 0.2$ (fm), and it looks as if it reaches an infinite value at $\delta_{20} = 0$. This behavior is consistent with a fact that the spherical nucleus exhibits very typical vibrational properties. In practice, however, an applicability limit of the SRM might be around there. On the other hand, the values of $\mu_{\beta_{20}}$ decrease as those of δ_{20} increase, and they seem to gradually come close to zero. The fact means that the deformed heavy nuclei have an ellipsoidal surface where the β_2-vibrational properties are not so important (strong) at least for the low-lying states.

- Figure 16-(b) presents the obtained values of γ_0 as a function of δ_{20}. It is a somewhat rough tendency, but the values surely decrease as δ_{20} parameters increase. The spherical nuclei apt to exhibit $\gamma_0 \sim 30°$, while the values of deformed heavy nuclei result in $\sim 10°$. As guessed from the context in Sec. 4.1, the quadrupole non-axiality seem to be related with the shell structure of neutrons and/or protons. This probable behavior can be seen as a systematic trend in this figure. In the next paragraph, we would examine the point more closely, and obtained findings are presented.

- Figure 16-(c) shows the estimated values of δ_{30} as a function of δ_{20}. We can see the behavior of the equilibrium G.S. octupole deformation mentioned in Sec. 4.1 as a systematic trend. First, the values increase with δ_{20}. They take a maximum at $\delta_{20} \sim 1.0$ (fm), and then gradually decline as the value of δ_{20} increase. Also, the values of those two parameters tend to be almost same up to ~ 1.0 (fm). The phenomenon indicates that the large octupole equilibrium deformation is difficult to be formed. It is interesting that the parameter exhibits a limiting length $\delta_{30} \sim 1.0$. By contrast, the quadrupole and the octupole equilibrium deformations are almost comparable in magnitude at lengths lower than ~ 1.0 (fm).

- Figure 16-(d) illustrates the results for the octupole softness constant μ_ϵ as a function of δ_{20}. Any clear systematic tendencies are not seen. It might be due to a poor predictive power of the

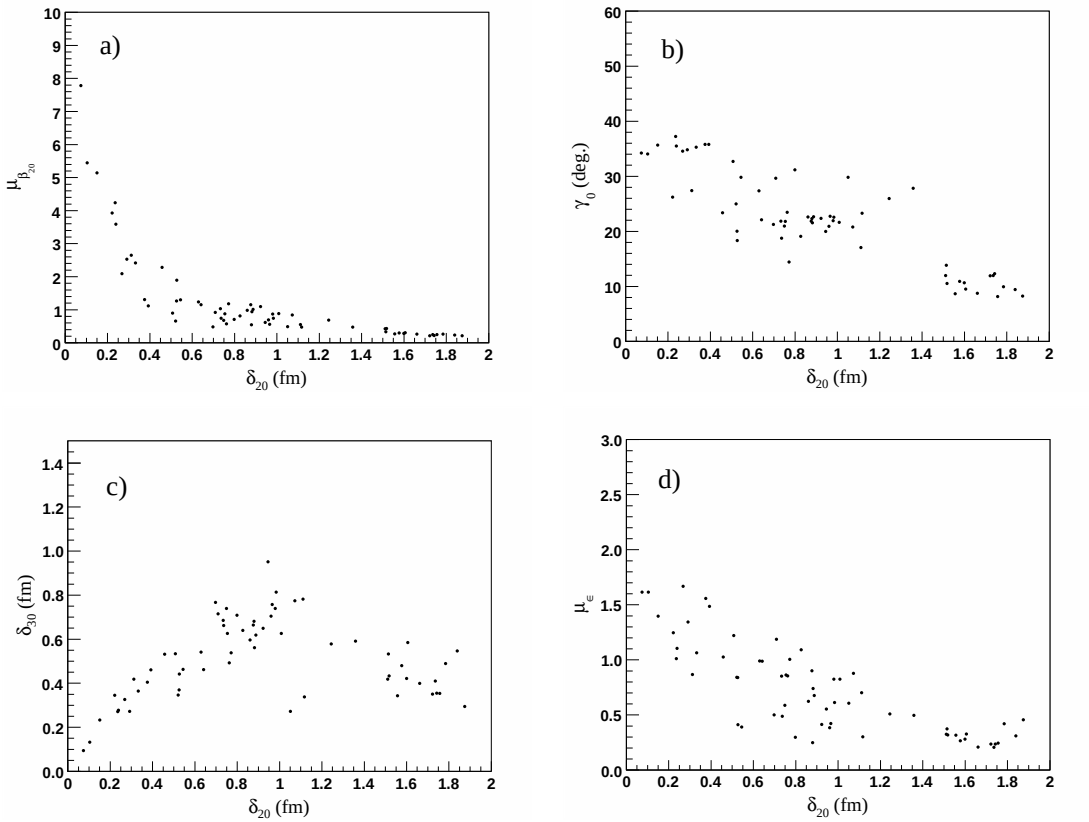

Fig. 16: Variations of major SRM Hamiltonian parameters against quadrupole deformation length $\delta_{20}(= 1.21A^{1/3}\beta_{20})$: a) Quadrupole softness parameter $\mu_{\beta_{20}}$, b) Quadrupole non-axial deformation parameter γ_0, c) Octupole deformation length $\delta_{30}(= 1.21A^{1/3}\beta_{30})$ and d) Octupole softness parameter μ_ϵ

model and/or the experimental information. However, the values surely decrease as the increase of δ_{20} which is the similar trend of $\mu_{\beta_{20}}$. The values of μ_ϵ do not exhibit a divergent behavior at $\delta_{20} \sim 0$ unlike the trend of $\mu_{\beta_{20}}$. This fact implies that the closed and the spherical shells are not extremely involved with the octupole vibrational property as mentioned in Sec. 4.1

The value of $\gamma_0\beta_{20}$ (or $\gamma_0\delta_{20}$) is a more suitable measure to investigate the non-axial natures, since the quantity should express an absolute value of the equilibrium quadrupole asymmetric deformation. In **Fig. 17**-(a), the obtained $\gamma_0\beta_{20}$ values are plotted as a function of the quadrupole static deformation β_{20} for all nuclei studied in this work. We can see all data are positioned over a broad area, but they do not exceed $\gamma_0 \sim \pi/6$ (30°) line. And it seems that $\gamma_0 \sim \pi/6$ line behaves a limit of the quadrupole non-axial parameter. In spite of this, however, there exist many nuclei which exhibit the almost middle shape ($\gamma_0 \sim \pi/6$) over a wide β_{20} range. Those isotopes correspond to ^{60,64}Ni, $^{64-70}$Zn, ^{70,72}Ge, ^{74}Se, ^{86}Sr, ^{96,98,100}Mo, $^{116-124}$Sn, ^{130}Te and ^{194}Pt. They are re-plotted in **Fig. 17**-(b). It should be noted that those nuclei have a closed (sub-)shell cores of neutrons or protons. We can also find another group which are positioned slightly below the $\gamma_0 = \pi/6$ line as illustrated exclusively in **Fig. 17**-(c). It includes the isotopes such as ^{58}Fe, ^{62}Ni, ^{74,76}Ge, $^{76-82}$Se, ^{102}Ru, $^{104-110}$Pd, $^{106-116}$Cd, $^{122-128}$Te, ^{144}Nd, ^{148,150}Sm and ^{192}Os. Their neutron and/or proton numbers slightly deviate from the magic numbers. The remaining data are plotted in **Fig. 17**-(d). It is difficult to identify a clear trend in this case due to the lack of data and the complicated shell structures.

Figure. 18 presents the values of the quadrupole mass-parameters which are calculated with estimated parameters. The data of ^{12}C and ^{28,30}Si are taken from Refs.[1, 7], and they are plotted in this figure. As a global trend, the parameter grows as the mass number increases, while such a behavior was not seen in the octupole and hexadecapole mass-parameters. The local fluctuations visible are ascribed to the overall scale parameter $\hbar\omega_0$ as well as $\mu_{\beta_{20}}$ and β_{20}.

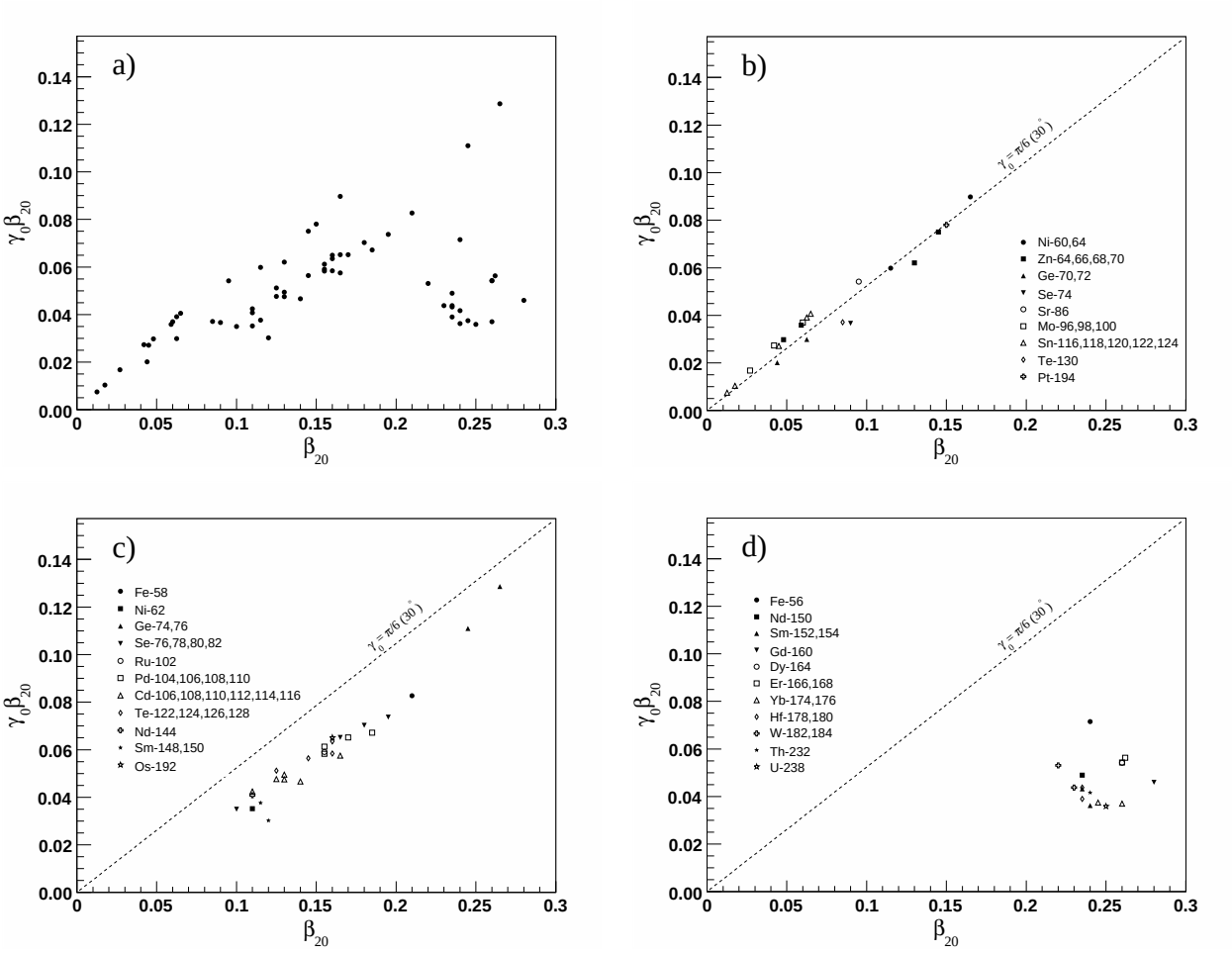

Fig. 17: Values of $\gamma_0\beta_{20}$ plotted as a function of β_{20}: a) for all nuclides, b) for nuclides of which γ_0-values are positioned around $\pi/6$ (30°) , c) for nuclides of which γ_0-values are slightly deviate from $\pi/6$, d) for nuclides of which γ_0-values are away from $\pi/6$

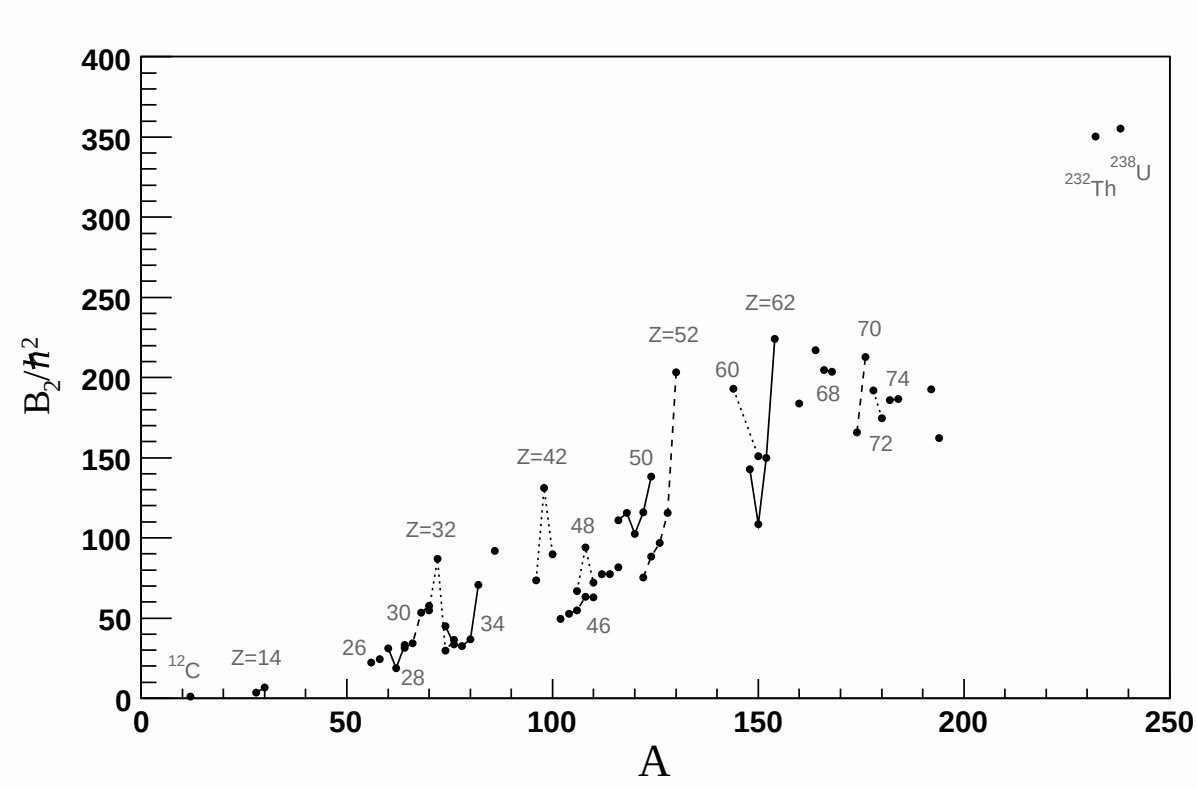

Fig. 18: Values of the quadrupole mass-parameter plotted as a function of the mass number A

5 Summary and Conclusions

The SRM-CC analyses were carried out for 63 even-even medium-heavy nuclei in order to see their individual behaviors and systematic trends of the collective natures. A complete SRM Hamiltonian parameter set was estimated for each nucleus by the combination of the level structure and the CC analysis for inelastically scattered protons. The obtained parameter values were expected to provide us with realistic and quantitative information on the equilibrium nuclear shape and rotational-vibrational characters, while it was difficult to obtain such knowledge just from experimental level and cross section data. It was found that values of the major parameters such as the softness and the equilibrium deformations showed us characteristics of each nucleus which were mostly ascribed to the shell structure effects. The obtained values of the effective quadrupole and octupole deformations were found to be very close to the experimental data. Besides, the equilibrium quadrupole deformation parameters also gave reasonable accordance with the mass-models results for deformed heavy nuclei. We confirmed that the SRM-CC analysis was an useful approach to represent collective behaviors of a nucleus. Systematic trends were also seen among the major Hamiltonian parameters. As well as the model itself, those findings are expected to give us one of useful guides for elaborate nuclear data calculation.

Acknowledgements

The authors would like to thank Drs. Yutaka Utsuno and Yosuke Toh of Japan Atomic Energy Agency (JAEA) for useful comments on the present work. We are also grateful to Dr. Jun-ichi Katakura of JAEA who promoted this study.

References

[1] S. Chiba, O. Iwamoto, Y. Yamanouchi, *et al.*, "Consistent Description of Collective Level Structure and Neutron Interaction Data for ^{12}C in the Framework of the Soft-rotator Model", *Nucl. Phys.*, **A624**, p.305 (1997).

[2] E. Sh. Soukhovitskiĭ, S. Chiba, O Iwamoto, *et al.*, "Programs OPTMAN and SHEMMAN version 8 (2004)", JAERI-Data/Code 2005-002 (2005).

[3] S. Chiba, O. Iwamoto, E. Sh. Sukhovitskiĭ, *et al.*, "Coupled-Channels Optical Potential for Interaction of Nucleons with ^{12}C Up to 150 MeV in the Soft-Rotator Model", *J. Nucl. Sci. Technol*, **37**, p.498 (2000).

[4] E. Sh. Sukhovitskiĭ, Y. -O. Lee, J. Chang, *et al.*, "Nucleon Interaction with ^{58}Ni up to 150 MeV Studied in the Coupled-Channels Approach Based on the Soft-Rotator Nuclear Structure Model", *Phys. Rev.*, **C62**, p.044605 (2000).

[5] E. Sh. Sukhovitskiĭ, S. Chiba, J. -Y. Lee, *et al.*, "Nuclear Level Structure, B(E2) Gamma-Transitions and Nucleon Interaction Data for ^{56}Fe by a Unified Soft-Rotator Model and Couple-Channels Framework", *J. Nucl. Sci. Technol*, **39**, p.816 (2002).

[6] E. Sh. Sukhovitskiĭ, S. Chiba, J. -Y. Lee, *et al.*, "Analysis of Nucleon Scattering Data of ^{52}Cr with a Coupling Scheme Built with the Soft-rotator Model", *J. Nucl. Sci. Technol*, **40**, p.69 (2003).

[7] W. Sun, Y. Watanabe, E. Sh. Sukhovitskiĭ, *et al.*, "Coupled-Channels Analysis of Nucleon Interaction Data of ^{28,30}Si up to 200 MeV Based on the Soft Rotator Model", *J. Nucl. Sci. Technol*, **40**, p.635 (2003).

[8] S. Kunieda, S. Chiba, K. Shibata, *et al.*, "Extensive Study of the Soft-Rotator Model Hamiltonian Parameters for Medium and Heavy Even-Even Nuclei", *J. Nucl. Sci. Technol*, **46**, p.914 (2009).

[9] S. Kunieda, S. Chiba, K. Shibata, *et al.*, "Systematical nucleon-induced optical model analysis for medium and heavy nuclei with coupled-channel framework", *Proc. of Int. Conf. Nuclear Data for Science and Technology, April 22-27, 2007, Nice, France*, EDP Sciences, 2008, pp.227-230.

[10] A. S. Davydov and A. A. Chaban, "Rotation-vibration Interaction in Non-axial Even Nuclei", *Nucl. Phys.*, **20**, p.499 (1960).

[11] Yu. V. Porodzinskiĭ and E. Sh. Sukhovitskiĭ, "Incorporating Hard Hexadecapole Modes in a Phenomenological Collective Nuclear Model with Five Dynamical Variables", *Yad. Fiz.*, **55**, p.2368 (1992).

[12] Yu. V. Porodzinskiĭ and E. Sh. Sukhovitskiĭ, "Analysis of Neutron Scattering by Even-Even Nuclei with Allowance for Dynamical Octupole Deformations", *Yad. Fiz.*, **59**(2), p.247 (1996).

[13] S. Kunieda, S. Chiba, K. Shibata, *et al.*, "Coupled-channels Optical Model Analyses of Nucleon-induced Reactions for Medium and Heavy Nuclei in the Energy Region from 1keV to 200 MeV", *J. Nucl. Sci. Technol*, **44**, p.838 (2007).

[14] P. J. Van Hall, J. P. M. G. Melssen, S. D. Wassenaar, *et al.*, "Scattering of Polarized Protons by Iron and Nickel Isotopes", *Nucl. Phys.*, **A291**, p.63 (1977).

[15] G. S. Mani, "Spin Assignments to Excited States of ^{56}Fe Using Inelastic Proton Scattering", *Nucl. Phys.*, **A165**, p.225 (1971).

[16] J. Takamatsu, T. Nakagawa, A. Terakawa, *et al.*, "Quadrupole Mixed-Symmetry States in ^{56}Fe", *J. Phys. (Paris)*, **55**, Suppl. C6, p.423 (1990).

[17] R. De Leo, H. Akimune, N. Blasi, *et al.*, "Isospin Character of Low-Lying States in ^{56}Fe", *Phys. Rev.*, **C53**, p.2718 (1996).

[18] G. S. Mani, "Spin Assignments to Excited States of ^{58}Fe Using Inelastic Scattering of 50 MeV Protons", *Nucl. Phys.*, **A169**, p.194 (1971).

[19] N. Lingappa and G. W. Greenlees, "Inelastic Scattering of 40-MeV Protons by ^{58}Ni58 and ^{60}Ni and Analysis in Coupled Channels", *Phys. Rev.*, **C2**, p.1329 (1970).

[20] A. Ingemarsson, T. Johansson, G. Tibell, "Elastic and Inelastic Scattering of 178 MeV Protons from ^{58}Ni and ^{60}Ni", *Nucl. Phys.*, **A365**, p.426 (1981).

[21] P. J. van Hall, S. D. Wassenaar, S. S. Klein, *et al.*, "Scattering of Polarized Protons by Ni, Sr, Cd, In and Sn Isotopes: II. Inelastic scattering - collective analysis", *J. Phys.*, **G15**, p.199 (1989).

[22] W. H. L. Moonen, J. H. A. M. Krabbenborg, H. P. Offermans, *et al.*, "Scattering of 20.4 MeV Polarized Protons from Even-Mass Zinc Isotopes", *J. Phys.*, **G19**, p.1191 (1993).

[23] W. H. Tait and V. R. W. Edwards, "A Study of 30 MeV Proton Inelastic Scattering from Isotopes of Molybdenum and Zinc", *Nucl. Phys.*, **A203**, p.193 (1973).

[24] M. Calderbank, E. J. Burge, V. E. Lewis, *et al.*, "The Elastic and Inelastic Scattering of 50 MeV Protons by ^{64}Zn, ^{66}Zn, ^{68}Zn and ^{70}Zn", *Nucl. Phys.*, **A105**, p.601 (1967).

[25] K. Yagi, Y. Saji, Y. Ishizaki, *et al.*, "The $L = 3$ and 4 Transitions in Inelastic Scattering of Protons from ^{66}Zn", *Nucl. Phys.*, **A132**, p.690 (1969).

[26] W. H. L. Moonen, P. J. van Hall, S. S. Klein, *et al.*, "Polarized-Proton Scattering by Even-Mass Germanium and Selenium Isotopes at 22 MeV Incident Energy", *J. Phys.*, **G19**, p.635 (1993).

[27] J. P. Delaroche, R. L. Varner, T. B. Clegg, *et al.*, "Structure of Low-Lying States of ^{76,78,80,82}Se Deduced from $(\vec{p}, p')$ Scattering at 16 MeV", *Nucl. Phys.*, **A414**, p.113 (1984).

[28] K. Ogino, "^{74,76,78,80,82}Se by inelastic scattering of 64.8 MeV protons", *Phys. Rev.*, **C33**, p.71 (1986).

[29] S. J. Burger and G. Heymann, "Alpha-Particle and Proton Scattering from Even Mass Molybdenum Isotopes", *Nucl. Phys.*, **A243**, p.461 (1975).

[30] H. F. Lutz, D. W. Heikkinen, W. Bartolini, "Proton Inelastic Scattering from the Five Stable, Even-Mass Isotopes of Molybdenum", *Phys. Rev.*, **C4**, p.934 (1971).

[31] E. Fretwurst, G. Lindstrom, K. F. von Reden, *et al.*, "Scattering of 25.6 MeV Protons on ^{94}Mo, ^{94}Mo and ^{100}Mo", *Nucl. Phys.*, **A468**, p.247 (1987).

[32] E. Cereda, M. Pignanelli, S. Micheletti, *et al.*, "Proton Scattering on $A = 92 - 116$ Nuclei with Extended Optical Models and the Interacting Boson Approximation", *Phys. Rev.*, **C26**, p.1941 (1982).

[33] M. Pignanelli, S. Micheletti, E. Cereda, *et al.*, "Proton Scattering on ^{100}Mo and ^{112}Cd and the Interacting Boson Approximation", *Phys. Rev.*, **C29**, p.434 (1984).

[34] Y. Aoki, H. Iida, K. Hashimoto, *et al.*, "Elastic and Inelastic Scattering of Polarized Protons from the Isotopes ^{104,106,108,110}Pd", *Nucl. Phys.*, **A394**, p.413 (1983).

[35] M. Koike, T. Suehiro, K. Pingel, *et al.*, "Elastic and Inelastic Scattering of 52 MeV Protons from ^{106}Pd, ^{108}Pd and ^{110}Pd", *Nucl. Phys.*, **A248**, p.237 (1975).

[36] R. M. A. L. Petit, B. W. van der Pluym, P. J. van Hall, *et al.*, "Scattering of 22.3 MeV Polarized Protons from the Even-Mass Cadmium Isotopes $^{106-116}Cd$", *J. Phys.*, **G20**, p.1955 (1994).

[37] S. Kailas, P. P. Singh, D. L. Friesel, *et al.*, "Excitation of Low-Lying Levels and Giant Multipole Resonances in ^{92}Zr, ^{120}Sn, and ^{208}Pb by Inelastic Scattering of 104 MeV Polarized Protons", *Phys. Rev.*, **C29**, p.2075 (1984).

[38] P. D. Cottle, S. M. Aziz, K. W. Kemper, *et al.*, "Proton Inelastic Scattering on the Transitional Nucleus ^{144}Nd", *Phys. Rev.*, **C43**, p.59 (1991).

[39] M. Pignanelli, N. Blasi, S. Micheletti, *et al.*, "Octupole Excitations in Vibrational Nuclei and the sdf Interacting Boson Model", *Nucl. Phys.*, **A519**, p.567 (1990).

[40] T. Kruse, W. Makofske, H. Ogata, *et al.*, "Elastic and Inelastic Proton Scattering from Heavy Collective Nuclei", *Nucl. Phys.*, **A169**, p.177 (1971).

[41] A. Guterman, D. L. Hendrie, P. H. Debenham, *et al.*, "Inelastic Scattering of 66.5 MeV Protons from ^{148}Sm and ^{154}Sm", *Phys. Rev.*, **C39**, p.1730 (1989).

[42] T. Ichihara, H. Sakaguchi, M. Nakamura, *et al.*, "Inelastic Proton Scattering Exciting the γ-Vibrational Band in Deformed Nuclei ($152 \leq A \leq 192$) at 65 MeV and the Systematics of the Hexadecapole (Y_{42}) Strength of the γ-Vibration", *Phys. Rev.*, **C36**, p.1754 (1987).

[43] C. H. King, G. M. Crawley, Jr. J. A. Nolen, *et al.*, "Extraction of Deformation Parameters from Inelastic Proton Scattering", *Proc. Int. Conf. on Nuclear Structure, Tokyo, 5-10 Sep 1977*, p.564 (1978).

[44] T. Ichihara, H. Sakaguchi, M. Nakamura, *et al.*, "Multipole Moments of ^{166}Er, ^{168}Er, ^{174}Yb, and ^{176}Yb from 65 MeV Polarized Proton Inelastic Scattering and Density Dependence of the Effective", *Phys. Rev.*, **C29**, p.1228 (1984).

[45] O. Kamigaito, H. Sakaguchi, M. Nakamura, *et al.*, "Inelastic Scattering of Protons, ^{3}He, and ^{4}He at 30 MeV/Nucleon from ^{166}Er and ^{176}Yb and Quadrupole Moments of the Optical Potential", *Phys. Rev.*, **C45**, p.1533 (1992).

[46] H. Ogawa, H. Sakaguchi, M. Nakamura, *et al.*, "Inelastic Scattering of 65-MeV Polarized Protons from ^{178}Hf, ^{180}Hf, ^{182}W, and ^{184}W and Multipole Moments of the Optical Potential", *Phys. Rev.*, **C33**, p.834 (1986).

[47] R. Perrino, R. De Leo, A. D. Bacher, *et al.*, "Low-Lying Excitations in ^{176}Yb and ^{180}Hf from $(\vec{p}, p')$ Scattering at $E(p) = 98.4$ MeV", *Phys. Rev.*, **C45**, p.1017 (1992).

[48] F. T. Baker, A. Sethi, V. Penumetcha, *et al.*, "^{192}Os$(\vec{p}, p')$ Reaction at 135 MeV", *Nucl. Phys.*, **A501**, p.546 (1989).

[49] A. Sethi, F. T. Baker, G. T. Emery, *et al.*, "^{194,198}Pt$(\vec{p}, p')$ Reaction and the Interacting Boson Model", *Nucl. Phys.*, **A518**, p.536 (1990).

[50] L. F. Hansen, I. D. Proctor, D. W. Heikkinen, *et al.*, "Nuclear Deformation in the Actinide Region by Proton Inelastic Scattering", *Phys. Rev.*, **C25**, p.189 (1982).

[51] C. H. King, J. E. Finck, G. M. Crawley, *et al.*, "Multipole Moments of ^{154}Sm, ^{176}Yb, ^{232}Th, and ^{238}U from Proton Inelastic Scattering", *Phys. Rev.*, **C20**, p.2084 (1979).

[52] T. Ichihara, "Systematics of the Hexadecapole (Y_{42}) Strength of the γ-vibration in Deformed Nuclei ($152 \leq A \leq 192$) from Inelastic Scattering of Polarized Protons at 65 MeV", *Mem. Fac. Sci., Kyoto Univ., Ser. Phys. Astrophys., Geophys. Chem.*, **C37**, p.191 (1988).

[53] H. Sakaguchi, M. Nakamura, K. Hatanaka, *et al.*, "Elastic Scattering of 65 MeV Polarized Protons", *Phys. Rev.*, **C26**, p.944 (1982).

[54] Y. Toh, T. Czosnyka, M. Oshima, *et al.*, "Coulomb Excitation of ^{74}Ge Beam", *Eur. Phys. J*, **A9**, p.353 (2000).

[55] M. Sugawara, Y. Toh, T. Czosnyka, *et al.*, "Multiple Coulomb excitation of a ^{70}Ge beam and the interpretation of the 0_2^+ state as a deformed intruder", *Eur. Phys. J*, **A16**, p.409 (2003).

[56] L. Guo, J. A. Maruhn and P. -G. Reinhard, "Triaxiality and shape coexistence in germanium isotopes", *Phys. Rev.*, **C76**, p.034317 (2007).

[57] S. Raman, C. W. Nestor, and P. Tikkanen, "Transition Probability from the Ground to the First-Excited 2^+ State of Even-Even Nuclides", *At. Data Nucl. Data Tables*, **78**, p.1 (2001).

[58] T. Kibedi, R. H. Spear, "Reduced Electric-Octupole Transition Probabilities, $B(E3; 0_1^+ \rightarrow 3_1^-)$ - An Update", *At. Data Nucl. Data Tables*, **80**, p.35 (2002).

[59] P. Moller, J. R. Nix, W. D. Myers, *et al.*, "Nuclear Ground-State Masses and Deformations", *At. Data Nucl. Data Tables*, **59**, p.185 (1995).

[60] S. Goriely, M. Samyn, P. H. Heenen, *et al.*, "Hartree-Fock mass formulas and extrapolation to new mass data", *Phys. Rev.*, **C66**, p.024326 (2002).

[61] H. Koura, T. Tachibana, M. Uno, *et al.*, "Nuclidic Mass Formula on a Spherical Basis with an Improved Even-Odd Term", *Prog. Theor. Phys.*, **113**, p.305 (2005).

This is a blank page.

国際単位系（SI）

表１．SI 基本単位

基本量	SI 基本単位	
	名称	記号
長さ	メートル	m
質量	キログラム	kg
時間	秒	s
電流	アンペア	A
熱力学温度	ケルビン	K
物質量	モル	mol
光度	カンデラ	cd

表２．基本単位を用いて表されるSI組立単位の例

組立量	SI 基本単位	
	名称	記号
面積	平方メートル	m^2
体積	立法メートル	m^3
速さ，速度	メートル毎秒	m/s
加速度	メートル毎秒毎秒	m/s^2
波数	毎メートル	m^{-1}
密度，質量密度	キログラム毎立方メートル	kg/m^3
面積密度	キログラム毎平方メートル	kg/m^2
比体積	立方メートル毎キログラム	m^3/kg
電流密度	アンペア毎平方メートル	A/m^2
磁界の強さ	アンペア毎メートル	A/m
量濃度(a)，濃度	モル毎立方メートル	mol/m^3
質量濃度	キログラム毎立法メートル	kg/m^3
輝度	カンデラ毎平方メートル	cd/m^2
屈折率(b)	（数字の） 1	1
比透磁率(b)	（数字の） 1	1

(a) 量濃度（amount concentration）は臨床化学の分野では物質濃度（substance concentration）ともよばれる。
(b) これらは無次元量あるいは次元１をもつ量であるが、そのことを表す単位記号である数字の１は通常は表記しない。

表３．固有の名称と記号で表されるSI組立単位

組立量	SI 組立単位			
	名称	記号	他のSI単位による表し方	SI基本単位による表し方
平面角	ラジアン(b)	rad	1 (b)	m/m
立体角	ステラジアン(b)	sr(c)	1 (b)	m^2/m^2
周波数	ヘルツ(d)	Hz		s^{-1}
力	ニュートン	N		m kg s^{-2}
圧力，応力	パスカル	Pa	N/m^2	m^{-1} kg s^{-2}
エネルギー，仕事，熱量	ジュール	J	N m	m^2 kg s^{-2}
仕事率，工率，放射束	ワット	W	J/s	m^2 kg s^{-3}
電荷，電気量	クーロン	C		s A
電位差（電圧），起電力	ボルト	V	W/A	m^2 kg s^{-3} A^{-1}
静電容量	ファラド	F	C/V	m^{-2} kg^{-1} s^4 A^2
電気抵抗	オーム	Ω	V/A	m^2 kg s^{-3} A^{-2}
コンダクタンス	ジーメンス	S	A/V	m^{-2} kg^{-1} s^3 A^2
磁束	ウエーバ	Wb	Vs	m^2 kg s^{-2} A^{-1}
磁束密度	テスラ	T	Wb/m^2	kg s^{-2} A^{-1}
インダクタンス	ヘンリー	H	Wb/A	m^2 kg s^{-2} A^{-2}
セルシウス温度	セルシウス度(e)	℃		K
光束	ルーメン	lm	cd sr(c)	cd
照度	ルクス	lx	lm/m^2	m^{-2} cd
放射性核種の放射能(f)	ベクレル(d)	Bq		s^{-1}
吸収線量，比エネルギー分与，カーマ	グレイ	Gy	J/kg	m^2 s^{-2}
線量当量，周辺線量当量，方向性線量当量，個人線量当量	シーベルト(g)	Sv	J/kg	m^2 s^{-2}
酸素活性	カタール	kat		s^{-1} mol

(a)SI接頭語は固有の名称と記号を持つ組立単位と組み合わせても使用できる。しかし接頭語を付した単位はもはやコヒーレントではない。
(b)ラジアンとステラジアンは数字の１に対する単位の特別な名称で、量についての情報をつたえるために使われる。実際には、使用する時には記号rad及びsrが用いられるが、習慣として組立単位としての記号である数字の１は明示されない。
(c)測光学ではステラジアンという名称と記号srを単位の表し方の中に、そのまま維持している。
(d)ヘルツは周期現象についてのみ、ベクレルは放射性核種の統計的過程についてのみ使用される。
(e)セルシウス度はケルビンの特別な名称で、セルシウス温度を表すために使用される。セルシウス度とケルビンの単位の大きさは同一である。したがって、温度差や温度間隔を表す数値はどちらの単位で表しても同じである。
(f)放射性核種の放射能（activity referred to a radionuclide）は、しばしば誤った用語で"radioactivity"と記される。
(g)単位シーベルト（PV,2002,70,205）についてはCIPM勧告2（CI-2002）を参照。

表４．単位の中に固有の名称と記号を含むSI組立単位の例

組立量	SI 組立単位		
	名称	記号	SI 基本単位による表し方
粘度	パスカル秒	Pa s	m^{-1} kg s^{-1}
力のモーメント	ニュートンメートル	N m	m^2 kg s^{-2}
表面張力	ニュートン毎メートル	N/m	kg s^{-2}
角速度	ラジアン毎秒	rad/s	m m^{-1} s^{-1}=s^{-1}
角加速度	ラジアン毎秒毎秒	rad/s^2	m m^{-1} s^{-2}=s^{-2}
熱流密度，放射照度	ワット毎平方メートル	W/m^2	kg s^{-3}
熱容量，エントロピー	ジュール毎ケルビン	J/K	m^2 kg s^{-2} K^{-1}
比熱容量，比エントロピー	ジュール毎キログラム毎ケルビン	J/(kg K)	m^2 s^{-2} K^{-1}
比エネルギー	ジュール毎キログラム	J/kg	m^2 s^{-2}
熱伝導率	ワット毎メートル毎ケルビン	W/(m K)	m kg s^{-3} K^{-1}
体積エネルギー	ジュール毎立方メートル	J/m^3	m^{-1} kg s^{-2}
電界の強さ	ボルト毎メートル	V/m	m kg s^{-3} A^{-1}
電荷密度	クーロン毎立方メートル	C/m^3	m^{-3} sA
表面電荷	クーロン毎平方メートル	C/m^2	m^{-2} sA
電束密度，電気変位	クーロン毎平方メートル	C/m^2	m^{-2} sA
誘電率	ファラド毎メートル	F/m	m^{-3} kg^{-1} s^4 A^2
透磁率	ヘンリー毎メートル	H/m	m kg s^{-2} A^{-2}
モルエネルギー	ジュール毎モル	J/mol	m^2 kg s^{-2} mol^{-1}
モルエントロピー，モル熱容量	ジュール毎モル毎ケルビン	J/(mol K)	m^2 kg s^{-2} K^{-1} mol^{-1}
照射線量（X線及びγ線）	クーロン毎キログラム	C/kg	kg^{-1} sA
吸収線量率	グレイ毎秒	Gy/s	m^2 s^{-3}
放射強度	ワット毎ステラジアン	W/sr	m^4 m^{-2} kg s^{-3}=m^2 kg s^{-3}
放射輝度	ワット毎平方メートル毎ステラジアン	$W/(m^2 sr)$	m^2 m^{-2} kg s^{-3}=kg s^{-3}
酵素活性濃度	カタール毎立方メートル	kat/m^3	m^{-3} s^{-1} mol

表５．SI 接頭語

乗数	接頭語	記号	乗数	接頭語	記号
10^{24}	ヨタ	Y	10^{-1}	デシ	d
10^{21}	ゼタ	Z	10^{-2}	センチ	c
10^{18}	エクサ	E	10^{-3}	ミリ	m
10^{15}	ペタ	P	10^{-6}	マイクロ	μ
10^{12}	テラ	T	10^{-9}	ナノ	n
10^9	ギガ	G	10^{-12}	ピコ	p
10^6	メガ	M	10^{-15}	フェムト	f
10^3	キロ	k	10^{-18}	アト	a
10^2	ヘクト	h	10^{-21}	ゼプト	z
10^1	デカ	da	10^{-24}	ヨクト	y

表６．SIに属さないが、SIと併用される単位

名称	記号	SI 単位による値
分	min	1 min=60s
時	h	1h =60 min=3600 s
日	d	1 d=24 h=86 400 s
度	°	1°=(π/180) rad
分	’	1’=(1/60)°=(π/10800) rad
秒	”	1”=(1/60)’=(π/648000) rad
ヘクタール	ha	$1ha=1hm^2=10^4m^2$
リットル	L, l	$1L=11=1dm^3=10^3cm^3=10^{-3}m^3$
トン	t	$1t=10^3$ kg

表７．SIに属さないが、SIと併用される単位で、SI単位で表される数値が実験的に得られるもの

名称	記号	SI 単位で表される数値
電子ボルト	eV	$1eV=1.602\ 176\ 53(14)\times10^{-19}J$
ダルトン	Da	$1Da=1.660\ 538\ 86(28)\times10^{-27}kg$
統一原子質量単位	u	1u=1 Da
天文単位	ua	$1ua=1.495\ 978\ 706\ 91(6)\times10^{11}m$

表８．SIに属さないが、SIと併用されるその他の単位

名称	記号	SI 単位で表される数値
バール	bar	$1 bar=0.1MPa=100kPa=10^5Pa$
水銀柱ミリメートル	mmHg	1mmHg=133.322Pa
オングストローム	Å	$1 Å=0.1nm=100pm=10^{-10}m$
海里	M	1 M=1852m
バーン	b	$1 b=100fm^2=(10^{-12}cm)2=10^{-28}m^2$
ノット	kn	1 kn=(1852/3600)m/s
ネーパ	Np	SI単位との数値的な関係は、対数量の定義に依存。
ベル	B	
デジベル	dB	

表９．固有の名称をもつCGS組立単位

名称	記号	SI 単位で表される数値
エルグ	erg	$1 erg=10^{-7}$ J
ダイン	dyn	$1 dyn=10^{-5}$N
ポアズ	P	1 P=1 dyn s cm^{-2}=0.1Pa s
ストークス	St	1 St =$1cm^2$ s^{-1}=$10^{-4}m^2$ s^{-1}
スチルブ	sb	1 sb =1cd cm^{-2}=10^4cd m^{-2}
フォト	ph	1 ph=1cd sr cm^{-2} 10^4lx
ガル	Gal	1 Gal =1cm s^{-2}=$10^{-2}ms^{-2}$
マクスウェル	Mx	1 Mx = 1G cm^2=10^{-8}Wb
ガウス	G	1 G =1Mx cm^{-2} =10^{-4}T
エルステッド(c)	Oe	1 Oe ≙ $(10^3/4\pi)$A m^{-1}

(c) ３元系のCGS単位系とSIでは直接比較できないため、等号「 ≙ 」は対応関係を示すものである。

表10．SIに属さないその他の単位の例

名称	記号	SI 単位で表される数値
キュリー	Ci	$1 Ci=3.7\times10^{10}Bq$
レントゲン	R	$1 R=2.58\times10^{-4}C/kg$
ラド	rad	$1 rad=1cGy=10^{-2}Gy$
レム	rem	$1 rem=1 cSv=10^{-2}Sv$
ガンマ	γ	1γ=1 nT=10-9T
フェルミ		1フェルミ=1 fm=10-15m
メートル系カラット		1メートル系カラット = 200 mg = 2×10-4kg
トル	Torr	1 Torr = (101 325/760) Pa
標準大気圧	atm	1 atm = 101 325 Pa
カロリー	cal	1cal=4.1858J（「15℃」カロリー），4.1868J（「IT」カロリー）4.184J（「熱化学」カロリー）
ミクロン	μ	1 μ =1μm=10^{-6}m

（第8版，2006年改訂）

この印刷物は再生紙を使用しています